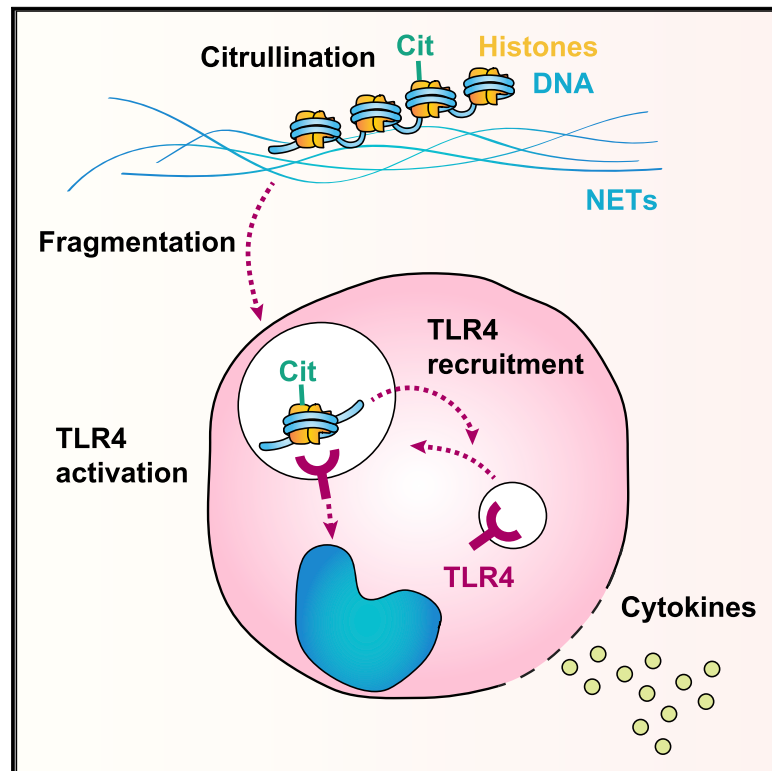


Histones, DNA, and Citrullination Promote Neutrophil Extracellular Trap Inflammation by Regulating the Localization and Activation of TLR4

Graphical Abstract



Authors

Theodora-Dorita Tsourouktsoglou, Annika Warnatsch, Marianna Ioannou, Dennis Hoving, Qian Wang, Venizelos Papayannopoulos

Correspondence

veni.p@crick.ac.uk

In Brief

Tsourouktsoglou et al. discuss how the pro-inflammatory capacity of neutrophil extracellular traps (NETs) depends on chromatin fragmentation, citrullination, and synergistic interactions between citrullinated histones and DNA. Histones are the primary pro-inflammatory agents, and DNA potentiates sub-lethal signaling by recruiting TLR4 to histone-containing endosomes.

Highlights

- Neutrophil extracellular trap chromatin is proinflammatory at sub-lethal concentrations
- Synergy between histones and DNA is critical for sub-lethal signaling
- Citrullination is dispensable for NETosis but potentiates histone-mediated signaling
- Histones activate TLR4, while DNA recruits TLR4 to histone-containing endosomes



Article

Histones, DNA, and Citrullination Promote Neutrophil Extracellular Trap Inflammation by Regulating the Localization and Activation of TLR4

Theodora-Dorita Tsourouktsoglou,¹ Annika Warnatsch,^{1,2} Marianna Ioannou,¹ Dennis Hoving,¹ Qian Wang,¹ and Venizelos Papayannopoulos^{1,3,*}

¹Antimicrobial Defense Laboratory, The Francis Crick Institute, 1 Midland Road, NW1 1AT London, UK

²Present address: Guy's Hospital, King's College, St. Thomas Street, SE1 9RT London, UK

³Lead Contact

*Correspondence: veni.p@crick.ac.uk

<https://doi.org/10.1016/j.celrep.2020.107602>

SUMMARY

Neutrophil extracellular traps (NETs) promote atherosclerosis by inducing proinflammatory cytokines, but the underlying mechanism remains unknown. NET DNA is immunogenic, but given the cytotoxicity of NET histones, it is unclear how it activates cells without killing them. Here, we show that histones, DNA, citrullination, and fragmentation synergize to drive inflammation below the histone cytotoxicity threshold. At low concentrations, nucleosomes induce cytokines, but high concentrations kill cells before cytokines are produced. The synergy between histones and DNA is critical for sub-lethal signaling and relies on distinct roles for histones and DNA. Histones bind and activate TLR4, whereas DNA recruits TLR4 to histone-containing endosomes. Citrullination is dispensable for NETosis but potentiates histone-mediated signaling. Consistently, chromatin blockade or PAD4 deficiency reduces atherosclerosis. Inflammation is also reduced in infected mice expressing GFP-tagged histones that block TLR4 binding. Thus, chromatin promotes inflammation in sterile disease and infection via synergistic mechanisms that use signals with distinct functions.

INTRODUCTION

Inflammation is the underlying cause of many chronic diseases. The mechanisms that regulate sterile inflammation are still poorly understood. Endogenous molecules, known as damage-associated molecular patterns (DAMPs), play a central role in inducing the cytokines that regulate the process. DAMPs can leak out of damaged cells, or they can be released by immune cells in a regulated manner. For example, the release of neutrophil extracellular traps (NETs) via programmed cell death induces inflammation in conditions such as gout and atherosclerosis (Muñoz et al., 2016; Warnatsch et al., 2015). NETs act as endogenous DAMPs that prime monocytes and macrophages to produce interleukin (IL)-1 β , a cytokine that promotes atherosclerosis along with other proinflammatory cytokines, such as IL-1 α and IL-6 (Warnatsch et al., 2015). The mechanisms that link NETs to the production of proinflammatory cytokines remain unknown.

NETs are pleiotropic molecules composed of decondensed chromatin and proteins such as the cathelicidin LL-37, S100A8, and high-mobility group protein 1 (HMGB1) that have been linked to inflammation (Lande et al., 2007, 2011; Tian et al., 2007; Ulas et al., 2017; Urban et al., 2009; Urbonaviciute et al., 2008; Vogl et al., 2007). Extracellular DNA is also thought to induce IL-1 β and type I interferons (IFNs) (Atianand and Fitzgerald, 2013) and is detected by Toll-like receptor (TLR)9, whereas cytosolic DNA in-

duces the intracellular sensors cGas/STING and AIM2 (Fernandes-Alnemri et al., 2009; Gaidt et al., 2017; Hornung et al., 2009; Ishikawa and Barber, 2008; Sun et al., 2013). Extracellular DNA is also internalized and detected by the cytosolic DNA receptors (Chamilos et al., 2012; Gehrke et al., 2013; Lood et al., 2016; Paludan and Bowie, 2013). Consistently, oxidation of NET DNA during NET formation increases its IFN-inducing capacity via the activation of cGas/STING (Lood et al., 2016). However, immune responses to endogenous DNA in its native nucleosomal state have not been characterized. This is a critical issue, because histones are cytotoxic *in vitro*, and their release in the circulation causes lethality in mouse models of sepsis and liver injury (Abrams et al., 2013; Huang et al., 2011; Kumar et al., 2015; Xu et al., 2009, 2011). TLRs are implicated in these phenotypes, and injection of pure recombinant histones drives chemokine expression and leukocyte recruitment (Huang et al., 2011; Westman et al., 2015; Xu et al., 2011). A recent study also identified a cytotoxic role for NET histones in fibrous cap erosion in atherosclerotic lesions (Silvestre-Roig et al., 2019). However, these phenotypes have predominantly been attributed to the cytotoxic properties of histones and their ability to disrupt cell membranes rather than to direct signaling activity (Huang et al., 2011; Silvestre-Roig et al., 2019; Xu et al., 2009, 2011). It is, therefore, unclear how chromatin DNA or other NET components might activate immune cells to produce cytokines without killing them.



In addition, NET chromatin bears unique post-translational modifications. During NET formation, histones become citrullinated by protein arginine deiminase 4 (PAD4), and this process is thought to be essential for NET formation (Leshner et al., 2012; Papayannopoulos et al., 2010; Wang et al., 2009). This unique modification has facilitated the identification of NETs *in vivo* (Branzk et al., 2014) but has also resulted in many studies interpreting the absence of citrullination as a lack in NET formation in PAD4-deficient animals without the use of additional NET markers. Moreover, the idea that citrullination is essential for NET formation has prohibited the investigation of a possible role for the modification in NET function.

In addition, little is known about the mechanisms that regulate cellular responses to NETs. Many TLR agonists act synergistically when presented together at low concentrations (Napolitani et al., 2005). Negative relationships between different classes of immune-sensing receptors have also been reported (Negishi et al., 2012). Together, these positive and negative relationships are thought to help refine immune responses (Tan et al., 2014). Synergy could be pivotal in the detection of NETs, as they contain an array of factors. Two NET proteins were shown to potentiate the detection of DNA by TLR9. LL-37 potentiates TLR9-mediated type-I IFN induction, whereas HMGB1 enhances TLR9 activation via the receptor for advanced glycation products (RAGE) (Lande et al., 2007; Tian et al., 2007). DNA-bound proteins also increase the uptake of nucleic acids (Bertheloot et al., 2016; Chamilos et al., 2012; Sirois et al., 2013). However, the physiological relevance of these synergistic interactions is not well defined.

Here, we investigate the pro-inflammatory NET components and their corresponding receptors and dissect the mechanisms that regulate the responses to NETs that ultimately drive atherogenesis. We report, for the first time, a role for histone citrullination in NET function, which helped uncover the importance of histones as major pro-inflammatory components in NETs. We demonstrate that the pro-inflammatory capacity of NETs depends on chromatin fragmentation, citrullination, and synergistic interactions of citrullinated histones with DNA, where histones are the primary pro-inflammatory agents and DNA potentiates signaling below the histone cytotoxicity threshold via a novel mechanism.

RESULTS

Citrullination Is Dispensable for NETosis in Atherosclerosis

Given the recent conflicting data surrounding the role of citrullination in NET formation, we sought to examine whether the phenotypes associated with PAD4 deficiency may be attributed to a role of citrullination in NET function (Claushuis et al., 2018; Kenny et al., 2017). First, we examined whether citrullination is implicated in NET formation induced by cholesterol crystals. Cl-amidine, a potent inhibitor of PADs, blocked histone citrullination effectively but failed to inhibit NET formation in human neutrophils induced by cholesterol crystals (Figure 1A). Measured in their native unfixed state, non-citrullinated NETs were equally decondensed. Un-citrullinated NETs contained typical NET markers such as neutrophil elastase (NE), myeloperoxidase

(MPO), calprotectin (S100A8) and proteolytically processed histone H3 (Figures 1B and 1C). However, NETs formed in the presence of Cl-amidine lacked citrullinated histone H3 as assessed by immunofluorescence microscopy and western immunoblotting. We also probed for NET formation in the atherosclerotic lesions of ApoE and ApoE/PAD4-deficient mice fed on a high-fat diet for 6 and 16 weeks. We stained for citrullinated histone H3 and additional NET markers such as Ly6G, which we have previously shown to colocalize with NETs (Warnatsch et al., 2015) and MPO. Chromatin was detected by staining with PL2-3, an antibody isolated from mice with spontaneous autoimmunity that recognizes epitopes in histones H2A and H2B and in DNA (Losman et al., 1992). We detected abundant NETs of similar size and distribution in both PAD4-deficient and PAD4-sufficient APO knockout mice (Figures 1D, 1E, and S1). The presence of non-citrullinated NETs in these lesions indicates that citrullination is not essential for NET formation in response to cholesterol crystals *in vitro* and in atherosclerotic lesions. Furthermore, it highlights the importance of additional chromatin markers for the detection of NETs in PAD4-deficient mice.

Nucleosomes and Citrullination Regulate Cytokine Production

Based on these findings, we hypothesized that citrullination could influence NET-mediated pathology by regulating the proinflammatory function of NETs. To test this hypothesis, we generated non-citrullinated NETs in the presence of Cl-amidine, solubilized them using restriction enzymes, and tested their capacity to induce IL-1 β expression in human primary blood monocytes. Non-citrullinated NET fragments exhibited a lower capacity to upregulate IL-1 β mRNA, IL-1 α , and IL-6 (Figures 2A and S2). At these NET concentrations, mRNA levels yielded by non-citrullinated NETs were comparable to those yielded from treatment of citrullinated NETs with DNase I (Figure S2). Given that histones are the major citrullinated proteins in NETs, this finding suggested that histones could be important in NET-mediated cytokine induction.

To address this question, we first examined whether purified nucleosomes were sufficient to activate monocytes. We purified native nucleosomes from granulocytic human leukemia 60 (HL-60) cells and generated different-size fragments with micrococcal nuclease (Mnase), which digests the inter-nucleosomal linker DNA without digesting any DNA that is directly bound to histones. Nucleosomes were potent inducers of IL-1 β , and their activating capacity increased as their fragment size decreased (Figure 2B). Activation was maximal with di-nucleosomes (0.4 kb) and mono-nucleosomes (0.2 kb) to levels comparable to those achieved with stimulation with lipopolysaccharide (LPS), suggesting that decondensation and partial nuclease processing are required for NET-mediated signaling. We also tested nucleosomes isolated from tissues of *CAG::H2B-EGFP* transgenic mice that express a H2B-EGFP fusion protein. These nucleosome-EGFP (EGFP-Nuc) preparations failed to induce cytokine expression, indicating that the presence of a bulky EGFP domain on nucleosomes interfered with their pro-inflammatory activity when compared with control nucleosomes of human or mouse origin (Figures 2B and 2C). This finding suggested that cytokine induction involved histone recognition by specific receptors that

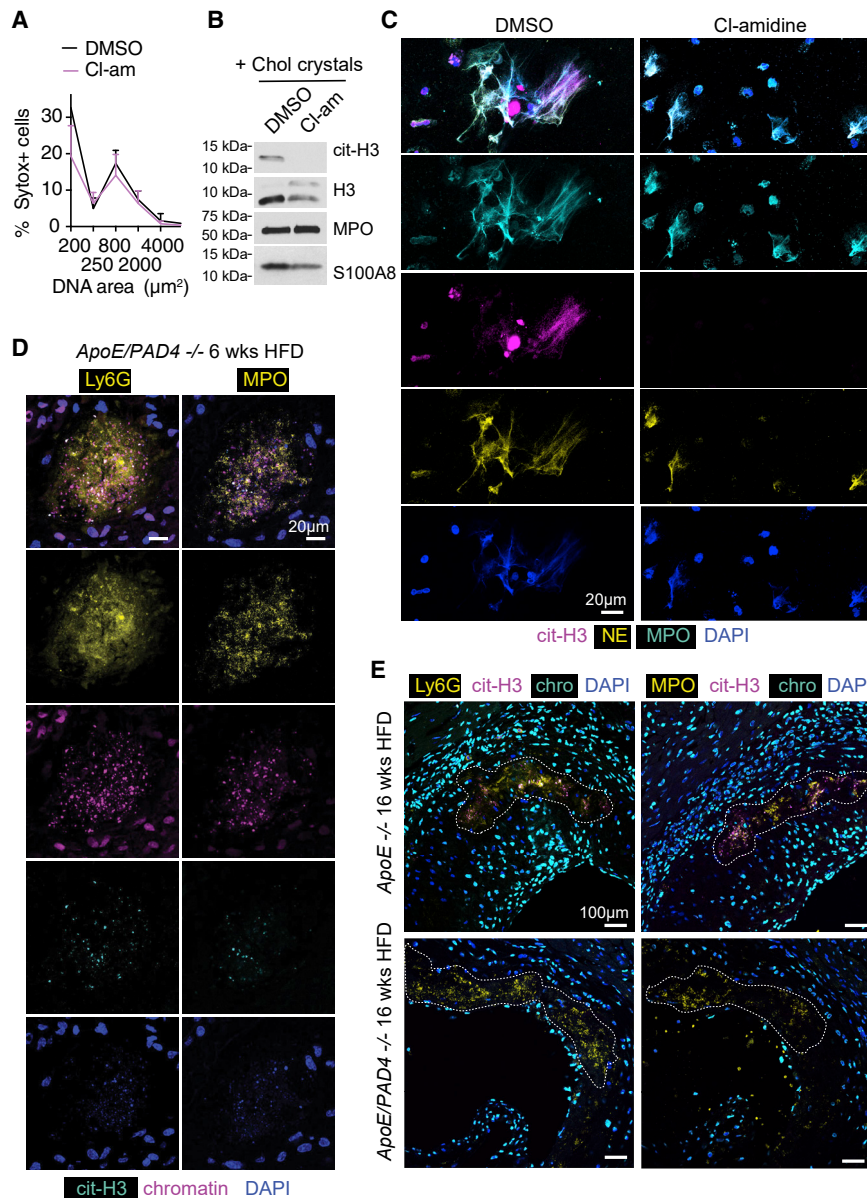


Figure 1. Histone Citrullination Is Not Required for NET Formation

(A) Quantification of NET formation detected by SYTOX Green in undisturbed primary human neutrophils, treated either with Cl-amidine (Cl-am) or with DMSO, and incubated for 4 h in the presence of cholesterol crystals. Extracellular chromatin decondensation was measured as an increase in extracellular DNA decondensation. The area of each SYTOX-stained nucleus is measured by microscopy and plotted as a frequency of SYTOX-positive dead cells falling within a range of nuclear areas. Data are represented as mean \pm SD.

(B) Western immunoblotting of NET preparations as in (A) stained for the NET markers cit-H3, H3, MPO, and S100A8.

(C) Cells from (A) immunostained for citrullinated histone H3 (cit-H3, magenta), myeloperoxidase (MPO, cyan), neutrophil elastase (NE, yellow), and DNA (DAPI, blue). Scale bar, 20 μ m. (D) Representative micrographs of consecutive aortic sections (left and right columns) from ApoE/PAD4-deficient animals after 6 weeks on a high-fat diet, fluorescently immunostained for the neutrophil marker Ly6G (yellow, left panel), which is also found in NETs; the anti-chromatin PL2-3 antibody (magenta); antibodies against citrullinated histone H3 (cit-H3, cyan); MPO (yellow, right panel); and DAPI (blue). Scale bars, 20 μ m.

(E) NET areas (outlined by dotted lines) in representative micrographs of consecutive aortic sections (left and right panels) from ApoE-deficient (top row) and ApoE/PAD4-deficient (bottom row) animals after 16 weeks on a high-fat diet, fluorescently immunostained for the neutrophil marker Ly6G (yellow, left column); the anti-chromatin PL2-3 antibody (magenta); antibodies against citrullinated histone H3 (cit-H3, cyan); MPO (yellow, right column); and DAPI (blue). Scale bars, 100 μ m. Data in (A), (B), and (C) are representative of three independent experiments.

was disrupted by EGFP rather than non-specific cytotoxicity. These results allowed us to investigate genetically whether histones promote inflammation *in vivo*. Given that H2B-EGFP-bearing nucleosomes did not exhibit proinflammatory activity *in vitro*, we used CAG::H2B-EGFP mice as a genetic tool to examine whether histones play a role in the induction of inflammation during pulmonary fungal infection, which promotes NET release (Branzk et al., 2014). We detected lower IL-1 β concentrations in the bronchoalveolar lavage (BAL) of CAG::H2B-EGFP mice after 24 h of intratracheal infection with *C. albicans* (Figure 2D), in spite of the similar pulmonary fungal load (Figure 2E), suggesting that histones are important for the induction of this cytokine during acute fungal infection. Murine bone-marrow-derived macrophages (BMDMs) from CAG::H2B-EGFP mice responded to various proinflammatory agonists, including cit-H3

complexed with NET DNA, indicating that the reduction in IL-1 β *in vivo* was not due to lack of cellular sensitivity but was caused by interference of EGFP with the pro-inflammatory activity of chromatin (Figure 2F). These data suggested that extracellular chromatin is a potent pro-inflammatory agent.

Histones Bind and Activate TLR4

To determine which receptor is required to sense nucleosomes, we tested nucleosomes against murine BMDMs that were deficient in TLR4, TLR9, or the intracellular DNA receptor STING. The wild-type (WT), TLR9-deficient, and STING-deficient BMDMs responded potently to nucleosomes, whereas TLR4-deficient cells were completely unresponsive to nucleosomes (Figure 3A). Consistently, antibodies against TLR2 and TLR4 significantly reduced IL-1 β induction in human monocytes (Figure 3B). We also compared the blocking capacity of receptor-neutralizing antibodies to a monovalent Fab generated from

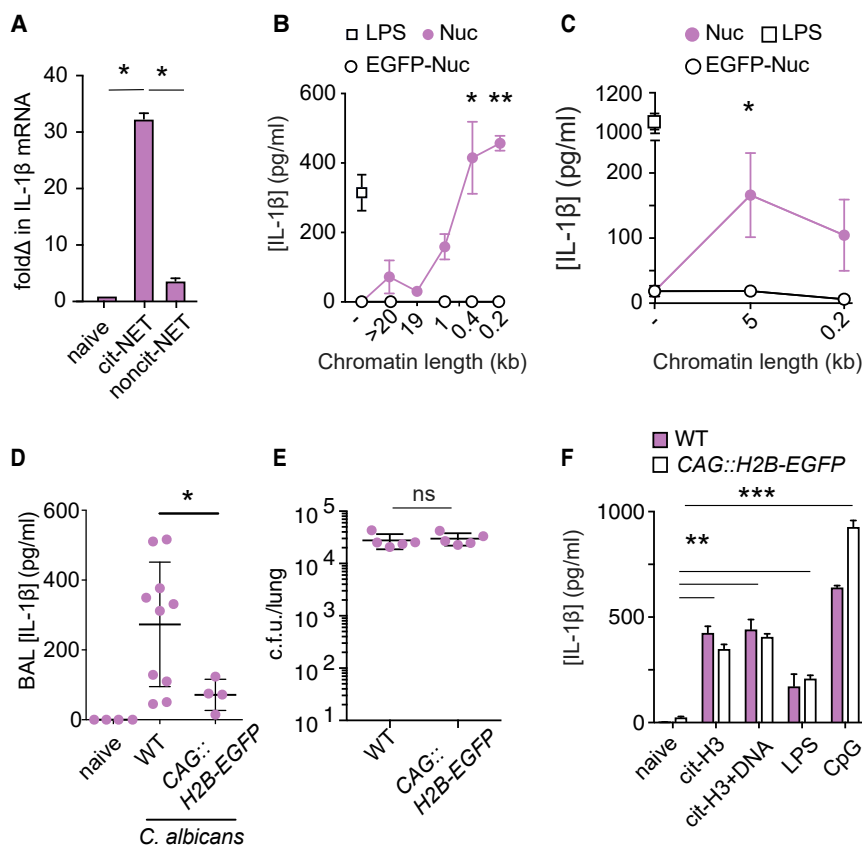


Figure 2. NET-Mediated Cytokine Induction Depends on Citrullinated Histones

(A) IL-1 β mRNA expression in human monocytes in response to NET fragments generated by restriction enzyme digest of cholesterol-crystal-stimulated neutrophils that were treated with either DMSO or Cl-amidine to generate citrullinated NETs (cit-NET) and non-citrullinated NETs (noncit-NET), respectively, analyzed by RT-PCR, and normalized to HPRT1 expression. Statistical analysis by the Mann-Whitney test. Data are represented as mean \pm SD and are representative of two individual stimulations per two donors.

(B) Total IL-1 β induced in untreated primary human monocytes or cells stimulated with a single concentration of nucleosomes (10^{-7} M) purified from neutrophil-like human leukemia-60 (HL-60) cells (Nuc) or from CAG::H2b-EGFP transgenic mice that overexpress a H2B-EGFP fusion protein (Nuc-EGFP), digested for different times with micrococcal nuclease (MNase) to generate different-size nucleosome fragments. For larger ranges, depicted chromatin sizes are the mean size of samples that contain a gradient of fragments centered around these values. Bacterial lipopolysaccharide (LPS) (0.5 ng/mL) was used as a positive control. Data are represented as mean \pm SD and are representative of three independent experiments. Statistical analysis by unpaired Student's t test.

(C) Total IL-1 β expression induced in human monocytes with nucleosomes at the indicated chromatin sizes purified from WT C57/Bl6 mice (Nuc) or CAG::H2B-EGFP mice (EGFP-Nuc) or LPS (0.5 ng/mL). Data are from three individual stimulations and are represented as mean \pm SD. Statistical analysis by unpaired Student's t test.

(D) IL-1 β in the BAL of WT and transgenic mice expressing an EGFP-tagged H2B fusion protein (CAG::H2B-EGFP) infected intratracheally with *C. albicans* for 24 h. Each point represents one animal, and data are represented as mean \pm SD. Statistical analysis by Mann-Whitney test.

(E) Fungal load in the lungs of mice in (D). Each point represents one animal, and data are represented as mean \pm SD. Statistical analysis by Mann-Whitney test.

(F) Total IL-1 β expression induced in murine BMDMs derived from either WT or CAG::H2B-EGFP mice in response to citrullinated histone H3 (10^{-7} M) alone or pre-complexed to NET DNA, LPS (0.5 ng/mL), or CpG (1 μ M). Data are represented as mean \pm SD. Statistical analysis by two-tailed t test.

* $p \leq 0.05$; ** $p \leq 0.01$; *** $p \leq 0.001$; ns, $p > 0.05$.

the PL2-3 anti-chromatin antibody against different mono-nucleosome concentrations. The reduction in pro-inflammatory capacity of mono-nucleosomes was comparable upon neutralization of TLR2/4 or histone blockade with the PL2-3 Fab (Figure 3C). TLR2/4 neutralization also blocked the activation of human monocytes when recombinant cit-H3 precomplexed to NET DNA was used as an agonist (Figure 3D). These data confirmed that TLR4 is required for histone-mediated IL-1 β induction in human monocytes.

We also tested the role of these receptors in sensing extracellular chromatin by activating a heterologous HEK-Blue TLR2 or TLR4 reporter cell system. In this system, TLR2 or TLR4-mediated nuclear factor κ B (NF- κ B) activation is measured by induction of the secreted embryonic alkaline phosphatase (SEAP). Mono-nucleosomes or recombinant citrullinated H3 protein activated HEK-Blue cells expressing TLR4, whereas cells expressing TLR2 or TLR9 exhibited very low sensitivity to histones, confirming that histones engage primarily TLR4 (Figures 3E, 3F, and S3A–S3D). Notably, EGFP nucleosomes failed to activate the TLR4 reporter cells, indicating that TLR4 is sensitive to

alterations in histone architecture, possibly involving steric hindrance by EGFP (Figure 3E).

To investigate whether histones physically interact with TLR4, we incubated HEK cells expressing either TLR2-hemagglutinin (HA) or TLR4-HA with recombinant citrullinated H3 or mono-nucleosomes. HA-tagged TLR4, but not TLR2, could be immunoprecipitated with a recombinant MBP-H3 fusion protein (Figure 3G) or antibodies against mono-nucleosomes (Figures 3H and 3I). Citrullination of nucleosomes using recombinant PAD4 increased binding to TLR4, suggesting a mechanism of action for the enhancement of NET-mediated signaling by this modification. Moreover, EGFP-Nuc preparations failed to bind TLR4, indicating that the inability of these molecules to induce IL-1 β is attributed to the lack of physical association with TLR4. Interestingly, *in vitro* citrullination of these EGFP-Nuc preparations reversed the binding inhibition exerted by EGFP. Therefore, changes in charge due to citrullination overcome the ability of EGFP to block TLR4, which indicates that citrullination can regulate histone-TLR4 interactions. Collectively our data demonstrate that native histones bind and activate TLR4. This

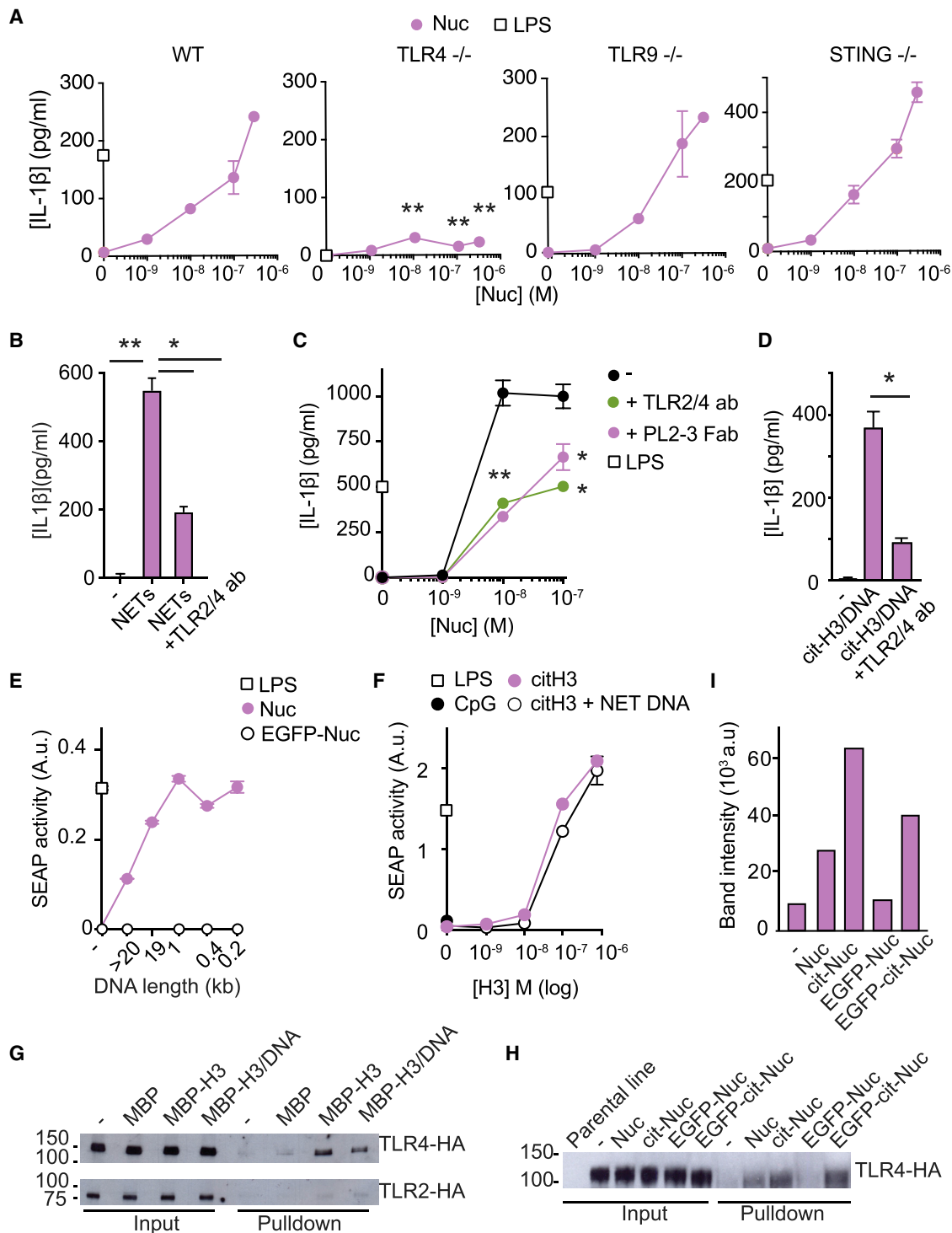


Figure 3. Histones Induce IL-1 β by Binding and Activating TLR4

(A) Total IL-1 β induced in BMDMs from WT or from TLR4^{-/-}, TLR9^{-/-}, or STING^{-/-} mice, incubated with increasing concentrations of mono-nucleosomes or LPS (0.5 ng/mL). Data are representative of three independent experiments and are represented as mean \pm SD. Statistical comparison of TLR4^{-/-} to WT via two-way ANOVA followed by Sidak's multiple comparison test.

(B) Total IL-1 β induced in untreated primary human monocytes or stimulated with cit-NETs alone or in the presence of neutralizing antibodies against TLR2 and TLR4. Statistical analysis by Mann-Whitney test. Data representative of three individual stimulations from two different donors and are represented as mean \pm SD.

(legend continued on next page)

interaction is not affected by their association to DNA but is potentiated by citrullination.

Histones Synergize with DNA in Cytokine Induction

Since NET DNA has also been implicated in inflammation, we assessed the role of DNA by treating chromatin preparations with DNase I or benzonase, two nucleases that degrade both inter-nucleosomal and histone-bound DNA to completely remove it from nucleosomes. These DNA-free nucleosomes lost their capacity to potently activate monocytes (Figure 4A). These data suggested that, in addition to histones, DNA was also required for potent cytokine induction in human monocytes. The magnitude of the decrease in cytokine induction upon complete DNA digestion suggested a potential synergistic relationship between DNA and histones.

To test whether synergy was involved, we performed titrations with purified NET DNA and recombinant histone H3. Histone H3 alone modestly activated monocytes at a concentration of 0.3 μ M. The addition of DNA at sub-threshold concentrations dramatically enhanced monocyte responsiveness to histone H3 (Figure 4B). Furthermore, citrullination of recombinant histones using a purified recombinant PAD4 enzyme further potentiated monocyte stimulation. We also found that monocytes failed to produce IL-1 β in response to concentrations of DNA up to 1.0 μ g/mL but that they were significantly sensitized to DNA stimulation in the presence of a non-activating concentration of histone H3 (Figure 4C). Therefore, synergy between histones and DNA confers the bulk of the pro-inflammatory activity of chromatin and NETs in human monocytes. Citrullination also influenced cytokine induction but played a less critical role as compared to DNA.

Given the ability of DNA to potentiate extracellular histone-mediated cytokine induction, we tested whether nucleosome DNA induced inflammatory signaling in our experimental conditions by examining the production of type I IFNs, which are known to be induced by DNA-mediated activation of TLR9 or STING. Purified citrullinated histone H3 alone or in the presence of NET DNA failed to induce type I IFNs (Figure 4D). Moreover, 10^{-7} M nucleosomes that were sufficient to potently induce IL-1 β failed to up-regulate IFN- α or IFN- β in human monocytes and murine BMDMs (Figures 4E and 4F). The lack of TLR9 activation by purified histones and NET DNA or mono-nucleosomes was also confirmed

using TLR9 reporter cell lines (Figures S3C and S3D). Therefore, these concentrations of extracellular NET DNA were unable to directly induce pro-inflammatory signaling in our experiments.

DNA Regulates Intracellular TLR4 Localization

Given that NET DNA did not influence histone binding to TLR4 in HEK cells, we hypothesized that the mechanism of synergy might involve changes in the cell biology of TLR4 in monocytes. Therefore, we examined the localization of TLR4 using flow cytometry by staining for intracellular, extracellular, and total TLR4. In human primary monocytes, TLR4 was completely absent from the cell surface and could only be detected intracellularly (Figure 5A). This led us to investigate whether DNA might promote the translocation of TLR4 to the cell surface to facilitate the recognition of extracellular chromatin. However, TLR4 localization remained intracellular after stimulation with NET DNA alone, histone H3, or a complex of the two (Figure 5B). Next, we investigated whether synergy might involve changes in intracellular TLR4 signaling. Consistent with this idea, inhibition of endosomal acidification with bafilomycin A reduced human monocyte responses to nucleosome stimulation (Figure 5C). To examine whether DNA induced changes in the intracellular TLR4 localization, we incubated human monocytes with MBP-H3 fusion protein alone or pre-complexed to NET DNA for 2 h. We stained for TLR4 and anti-MBP to visualize internalized extracellular histones and distinguish them from endogenous chromatin. In the presence of DNA, TLR4 was localized around 45% of the compartments containing internalized histone H3 (Figures 5D and 5E). Many of these compartments also sequestered Ras-related protein Rab-5 (Rab5), confirming that extracellular histones were being sequestered in early endosomes (Figure 5F). In the absence of DNA, TLR4 failed to translocate to histone-containing endosomes, suggesting that extracellular DNA exerted its synergistic effects by promoting the translocation of TLR4 to endosomes containing internalized histones.

Synergy Enables Sub-lethal Signaling

A synergistic relationship between different TLR agonists has been previously reported (Napolitani et al., 2005), but the physiological context of this phenomenon is not well defined. We reasoned that synergy may serve as a mechanism to enable cytokine

(C) Total IL-1 β induced in primary human monocytes upon titration of mono-nucleosomes alone or in the presence of antibodies against chromatin (PL2-3 Fab) and TLR2 and TLR4. Statistical analysis by two-tailed Student's t test. Data are representative of three independent experiments and are represented as mean \pm SD.

(D) Total IL-1 β induced in primary human monocytes stimulated with recombinant cit-H3 (0.03 μ M) and NET DNA (300 ng) in the presence or absence of anti-TLR2 and anti-TLR4 neutralizing antibodies. Statistical analysis by Mann-Whitney test. Data are representative of three independent experiments and are represented as mean \pm SD.

(E and F) TLR4-mediated NF- κ B activity assessed in a heterologous HEK-Blue cell system, by NF- κ B-driven induction of secreted embryonic alkaline phosphatase (SEAP). (E) TLR4 HEK-Blue reporter cells were treated with different fragments of purified HL-60 chromatin or mouse EGFP-tagged nucleosomes or LPS (0.5 ng/mL). (F) TLR4 HEK-Blue reporter cells were stimulated with LPS (0.5 ng/mL) or CpG (1 μ M) or recombinant citrullinated H3 alone or in complex with NET DNA. Data are representative of three (E) or five (F) independent experiments and are represented as mean \pm SD.

(G) HEK cells expressing TLR4-HA or TLR2-HA were incubated with recombinant H3 fused to maltose-binding protein (MBP-H3) alone or complexed to NET DNA. Cells were lysed, and interacting proteins were pulled down with amylose beads and immunoblotted with antibodies against HA. The total cell lysate (input) and the pull-down are depicted. Input was diluted 20 \times more than the pull-down.

(H) HEK cells expressing TLR4-HA were incubated alone (-) or with *in vitro* citrullinated or non-citrullinated human mono-nucleosomes or mouse EGFP-mono-nucleosomes. Lysates were immunoprecipitated using an antibody against histone H3 and immunoblotted with antibodies against HA. The total cell lysate (input) was diluted 20 \times more than the pull-down samples.

(I) Band intensities in (H) using ImageJ analysis.

*p \leq 0.05; **p \leq 0.01; ***p \leq 0.001; ns, p > 0.05.

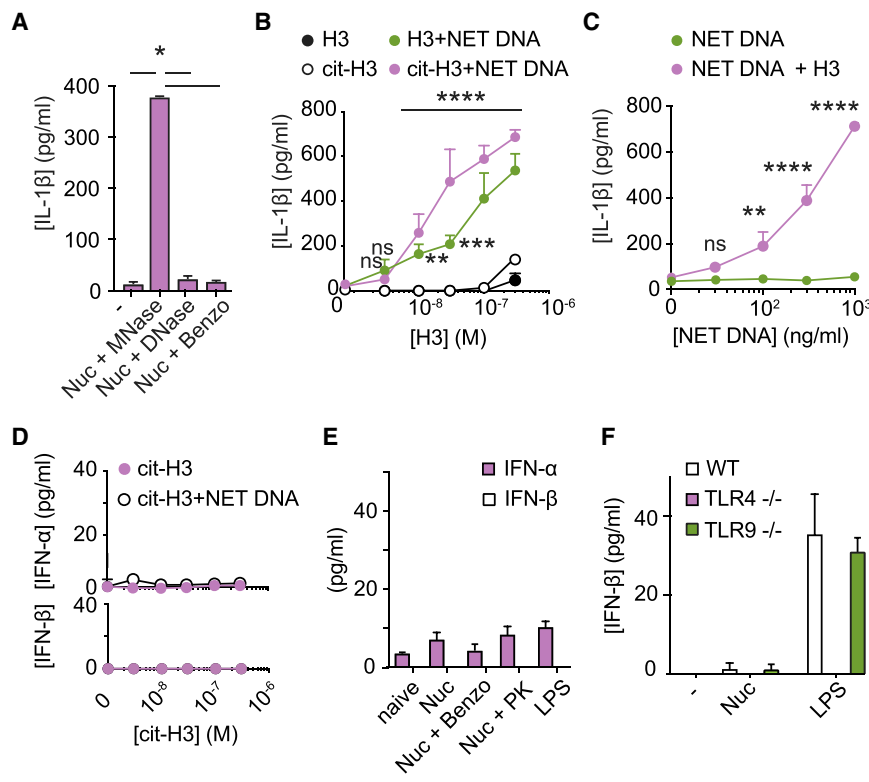


Figure 4. Synergy between DNA and Histones Enhances Cytokine Induction

(A) Total IL-1β induced in untreated primary human monocytes or stimulated with 10⁻⁷ M HL-60 mono-nucleosomes containing a 0.2 kb DNA fragment generated by MNase digestion (+MNase) or naked DNA-free mono-nucleosomes generated with DNase I (+DNase) or Benzonase (+Benzo). Statistical analysis by Mann-Whitney test. Data are representative of two independent stimulations per two donors and are represented as mean ± SD.

(B and C) Total IL-1β induced in primary human monocytes in the presence of increasing concentrations of either (B) recombinant histone H3 or *in vitro* citrullinated H3 (cit-H3), alone or in the presence of low concentrations of DNA purified from human NETs (NET DNA, 100 ng/mL), or (C) NET DNA in the presence of 10⁻⁷ M recombinant histone H3. Statistical analysis by two-way ANOVA followed by (B) Tukey's multiple comparisons test or (C) Sidak's multiple comparisons, comparing each double stimulation to its relevant single stimulant. Data are representative of at least (B) five independent experiments or (C) two independent stimulations in two independent experiments and are represented as mean ± SD.

(D) IFN-α and IFN-β protein in the lysate of primary human monocytes from (B).

(E) IFN-α and IFN-β of primary human monocytes stimulated with 0.5 μM mono-nucleosomes, alone or treated with proteinase K (PK) or Benzonase (Benzo), or LPS (0.5 ng/mL). Data are represented as mean ± SD.

(F) IFN-β protein in the supernatant of WT or of TLR4- or TLR9-deficient BMDMs stimulated with 0.5 μM mono-nucleosomes or LPS (0.5 ng/mL).

In (D)–(F), data are representative of two independent stimulations and are represented as mean ± SD. *p ≤ 0.05; **p ≤ 0.01; ***p ≤ 0.001; ****p ≤ 0.0001; ns, p > 0.05.

induction below the histone cytotoxicity threshold. Thus, we examined the relationship between mono-nucleosome uptake and cytotoxicity in human monocytes. We used EGFP-labeled nucleosomes that do not prime monocytes and monitored EGFP uptake and cell viability over time by flow cytometry (Figure 6A). We found that monocytes were viable and could tolerate mono-nucleosomes for up to 16 h at concentrations of 10⁻⁷ M, but all histone-containing cells died upon exposure to nucleosome concentrations of 5 × 10⁻⁷ M or higher (Figures 6A and 6B). By comparison, nucleosomes activated human monocytes at concentrations as low as 10⁻⁹ M, with stimulation peaking at concentrations of 10⁻⁸ M to 10⁻⁷ M (Figure 6C). Consistent with a rapid loss in viability, human monocytes failed to produce any IL-1β upon exposure to nucleosomes at a concentration of 10⁻⁶ M, which indicates that, from a technical standpoint, optimal chromatin concentration is critical in the detection of cytokine induction. Therefore, histone cytotoxicity suppresses pro-inflammatory responses at high chromatin concentrations, while the synergy between histones and DNA enables human monocytes to respond to chromatin at concentrations that are well below the cytotoxicity threshold.

Endogenous Histones Promote Atherosclerosis

To examine whether extracellular chromatin was a major driver of NET-induced inflammation during atherosclerosis, we tested

the effects of PAD4 deficiency and chromatin-blocking antibodies in a murine model of atherosclerosis. We treated female ApoE-deficient mice with either PL2-3 immunoglobulin G (IgG) or the Fab fragment. Treatment with the PL2-3 Fab antibody did not affect blood cholesterol and triglyceride concentrations (Figure S4), but markedly reduced atherosclerotic lesion size (Figures 7A and 7B). However, the full-length anti-chromatin PL2-3 antibody did not reduce plaque formation, suggesting either a lower efficiency in penetrating the arterial cell wall or the importance of the removal of the antibody effector function. By comparison, ApoE/PAD4-deficient animals exhibited an intermediate reduction in plaque size. Overall, plasma IL-1β concentrations were lower in mice receiving the PL2-3 Fab, but these differences were not statistically significant (Figure 7C). These findings suggested that extracellular chromatin is a major driver of local sterile inflammation that promotes atherosclerosis. To interrogate the basis of the differences in the *in vivo* efficacy against atherosclerosis between the full-length and the Fab version of the PL2-3, we compared their ability to block nucleosome-mediated induction of IL-1β in cultured murine BMDMs. The full-length antibody and the Fab fragment exhibited comparable capacity to block cytokine induction *in vitro*, indicating that the ineffectiveness of the full-length PL2-3 antibody is only relevant *in vivo* (Figure 7D). Interestingly, an antibody against histone H3 could not block the induction of IL-1β *in vitro*, indicating that

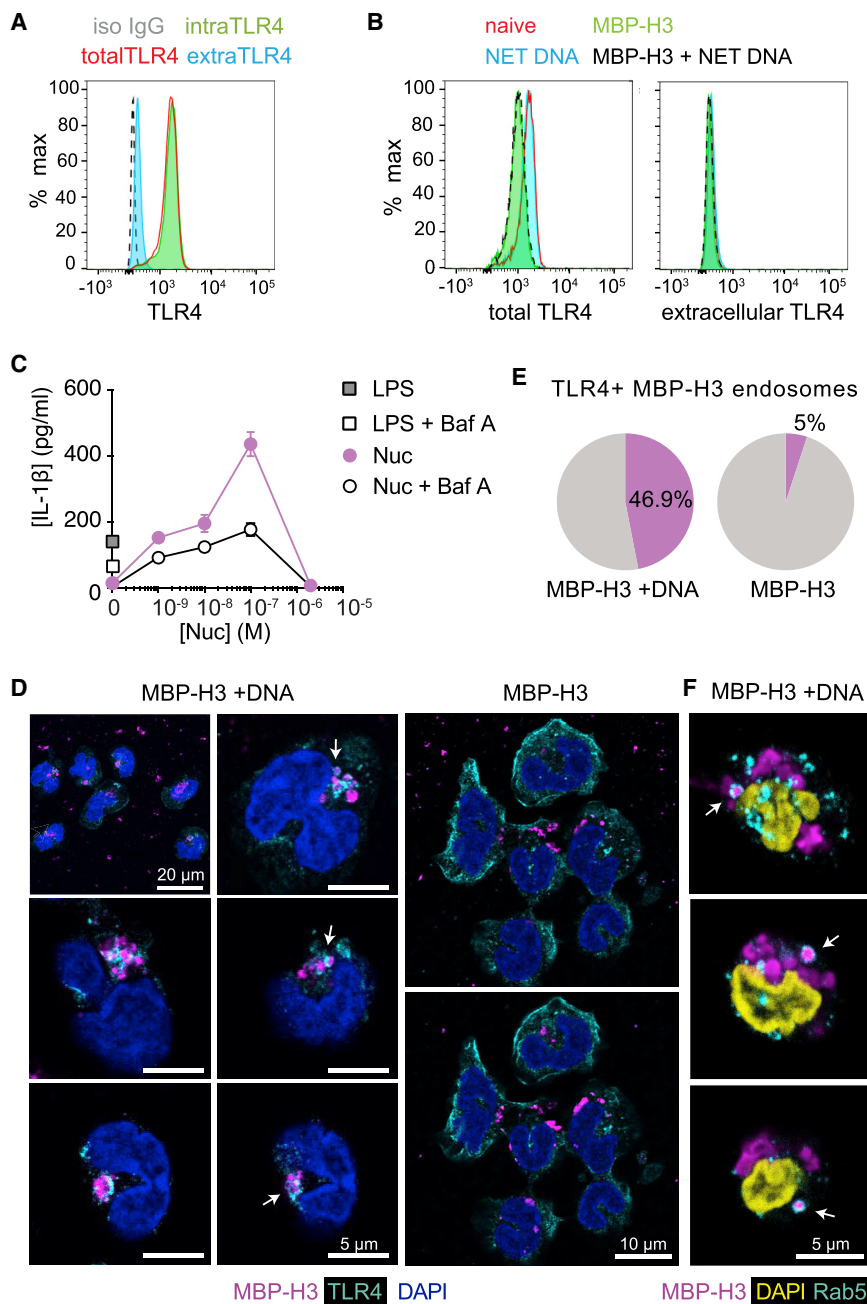


Figure 5. DNA Promotes Synergy by Promoting Intracellular TLR4 Translocation to Histone-Containing Endosomes

(A) Analysis of TLR4 localization in human monocytes by flow cytometry depicting cell-surface expression of extracellular TLR4 (extraTLR4, blue), intracellular TLR4 (intraTLR4, green), and total protein (totalTLR4, red).

(B) Total and extracellular TLR4 in human monocytes analyzed by flow cytometry after 2 h stimulations with NET DNA (blue, 300 ng/mL), histone H3 fused to MBP (MBP-H3, green, 0.5 μ M), or MBP-H3 bound to NET DNA (black).

(C) Total IL-1 β induced in human blood monocytes stimulated with LPS or mono-nucleosomes in the absence or presence of bafilomycin A. Data are represented as mean \pm SD.

(D) Representative immunofluorescence confocal micrograph series of human monocytes incubated for 2 h with recombinant histone H3 fused to maltose-binding protein (MBP), alone or pre-complexed with NET DNA, stained for DAPI (nuclear DNA, blue), MBP to detect exogenous histone H3 (magenta) and TLR4 (cyan). Top left panel in MBP-H3+DNA sample depicts a maximum projection of 5 sections from a single image (scale bar, 20 μ m). The other 5 panels depict higher magnification images of single confocal sections from cells in the top left panel (scale bars, 5 μ m). Arrows indicate TLR4 recruitment to MBP-H3-containing compartments. Both MBP-H3 micrographs are different z stack confocal sections from the same cells (scale bar, 10 μ m).

(E) Fraction of MBP-H3 containing endosomes that display TLR4 recruitment as in (D), enumerated from 25–30 cells per sample. A total of 99 endosomes accounted for MBP-H3 alone, and 147 accounted for MBP-H3 + NET DNA.

(F) Rab5-positive endosomes (arrows) in a z stack representative immunofluorescence confocal micrograph series of human monocytes incubated with recombinant histone H3 fused to MBP pre-complexed with NET DNA for 2 h and stained for DAPI (nuclear DNA, yellow), MBP to detect exogenous histone H3 (magenta) and Rab5 (cyan) (scale bar, 5 μ m).

chromatin-blocking efficiency may vary among different chromatin-targeting antibodies and may involve specific epitope recognition.

DISCUSSION

Our data indicate that endogenous externalized chromatin is a key driver of inflammation in sterile disease but can also amplify inflammation during infection. Chromatin components appear to have distinct modes of action that enable synergistic interac-

tions. Histones are the main signaling mediator that activates the transcription of IL-1 β in mononuclear cells by binding and activating TLR4. Instead, the contribution of chromatin DNA in direct immune signaling is limited by the histone cytotoxicity threshold. However, chromatin DNA serves a previously unknown function by regulating the cellular localization of intracellular TLR4 to promote TLR4 recruitment to endosomes containing internalized chromatin. We also excluded that DNA synergy could be due to avidity stemming from tethering multiple nucleosomes, since chromatin fragmentation increased its activation potential and DNA did not influence TLR4 reporter activity in cells that overexpress the receptor. This model differs from findings in plasmacytoid dendritic cells where proteins potentiate

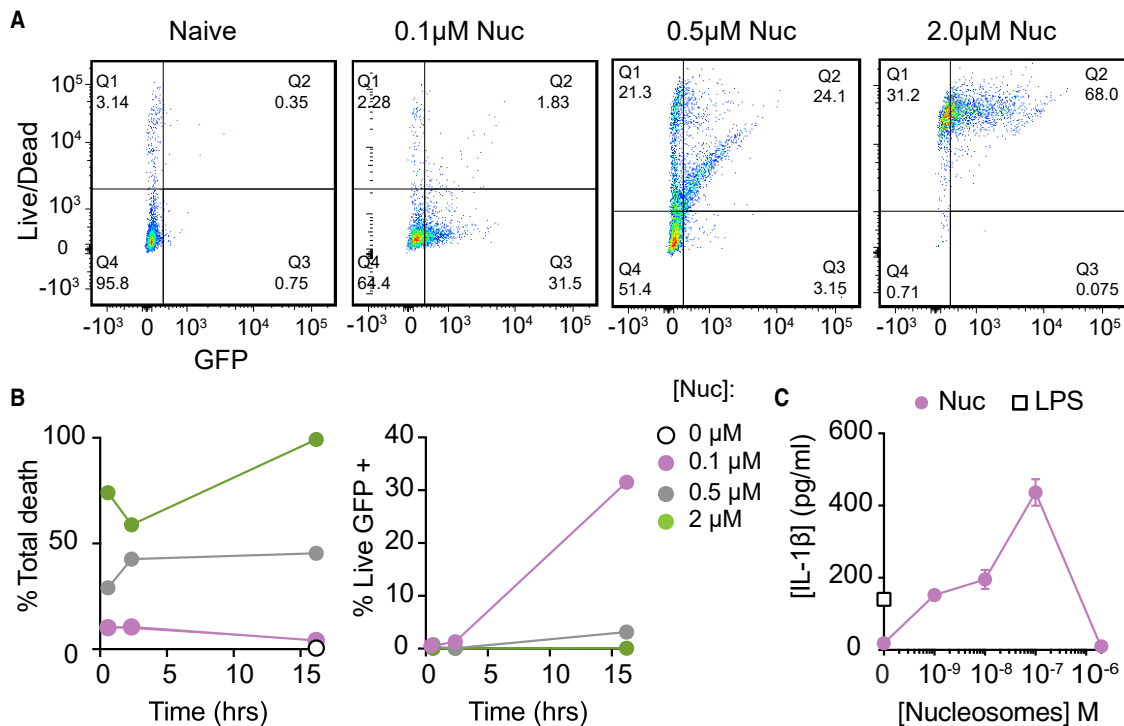


Figure 6. Histone-DNA Synergy Enables Cytokine Induction below the Histone Cytotoxicity Threshold

(A) Human monocytes incubated with purified EGFP-tagged mono-nucleosomes at the indicated concentrations for 2 h stained with a live/dead dye and analyzed by flow cytometry. Data are representative of three independent experiments.
 (B) Human monocytes incubated with purified EGFP-tagged mono-nucleosomes at the indicated concentrations for indicated time points as in (A). Time points depict percent total death or fraction of live GFP-positive cells over time for each concentration of nucleosomes. Data are representative of three independent experiments.
 (C) Total IL-1 β induced in human monocytes incubated with either LPS (55 pg/mL) or increasing concentrations of human mono-nucleosomes. Data are represented as mean \pm SD.

DNA-mediated signaling upstream of type I IFN expression (Lande et al., 2007).

Our model also provides a new concept in our understanding of the mechanisms that drive synergy between different TLR agonists. Prior work suggested that synergy between microbial TLR agonists is mediated by the enhanced activation of the extracellular signal-regulated kinase (ERK) and mitogen-activated protein kinase (MAPK) pathways (De Nardo et al., 2009). Another mechanism involves direct physical interaction between different receptors. For instance, DNA-bound HMGB1 recruits RAGE into a complex with TLR9 to enhance myeloid differentiation primary response 88 (MyD88) recruitment (Tian et al., 2007). However, it is conceptually difficult to explain the synergistic action between two cues that converge on the same downstream pathways via separate receptors. Instead, synergy can be easily achieved if the two activators play distinct roles in the signal transduction cascade, with one signal promoting receptor recruitment and the second signal triggering receptor activation. This mode of action provides a new paradigm for synergy among endogenous TLR agonists.

Moreover, in this instance, our data provide an explanation for the physiological role of synergy between cytotoxic DAMPs. The requirement for synergy serves to enable sub-lethal signaling by

weak agonists but also introduces opportunities for regulation. For example, circulating chromatin occurs in sepsis and other systemic inflammatory conditions (Xu et al., 2009). The requirement for DNA might serve to enable serum DNases to suppress the potent activation of blood monocytes by circulating chromatin via the degradation of DNA. Cells may also be able to tune their sensitivity to DAMPs by regulating the cellular localization of TLR4. Moreover, the model predicts that, at low concentrations, NETs are proinflammatory, while at high NET concentrations, histone cytotoxicity is likely to reduce inflammation. This mechanism may contribute to the anti-inflammatory effect of aggregated NETs in addition to the degradation of pro-inflammatory molecules by NET proteases (Leppkes et al., 2016; Schauer et al., 2014).

The requirement for chromatin fragmentation provides an additional layer for the regulation of inflammatory responses. NET decondensation and subsequent processing by endonucleases may allow immune cells to differentiate between chromatin originating from dead cells and chromatin from NETing neutrophils. The role of nucleases clearly depends on their ability to fragment chromatin partially or completely. Enzymes that fragment chromatin without degrading nucleosome-bound DNA enhance inflammation by generating pro-inflammatory mono-

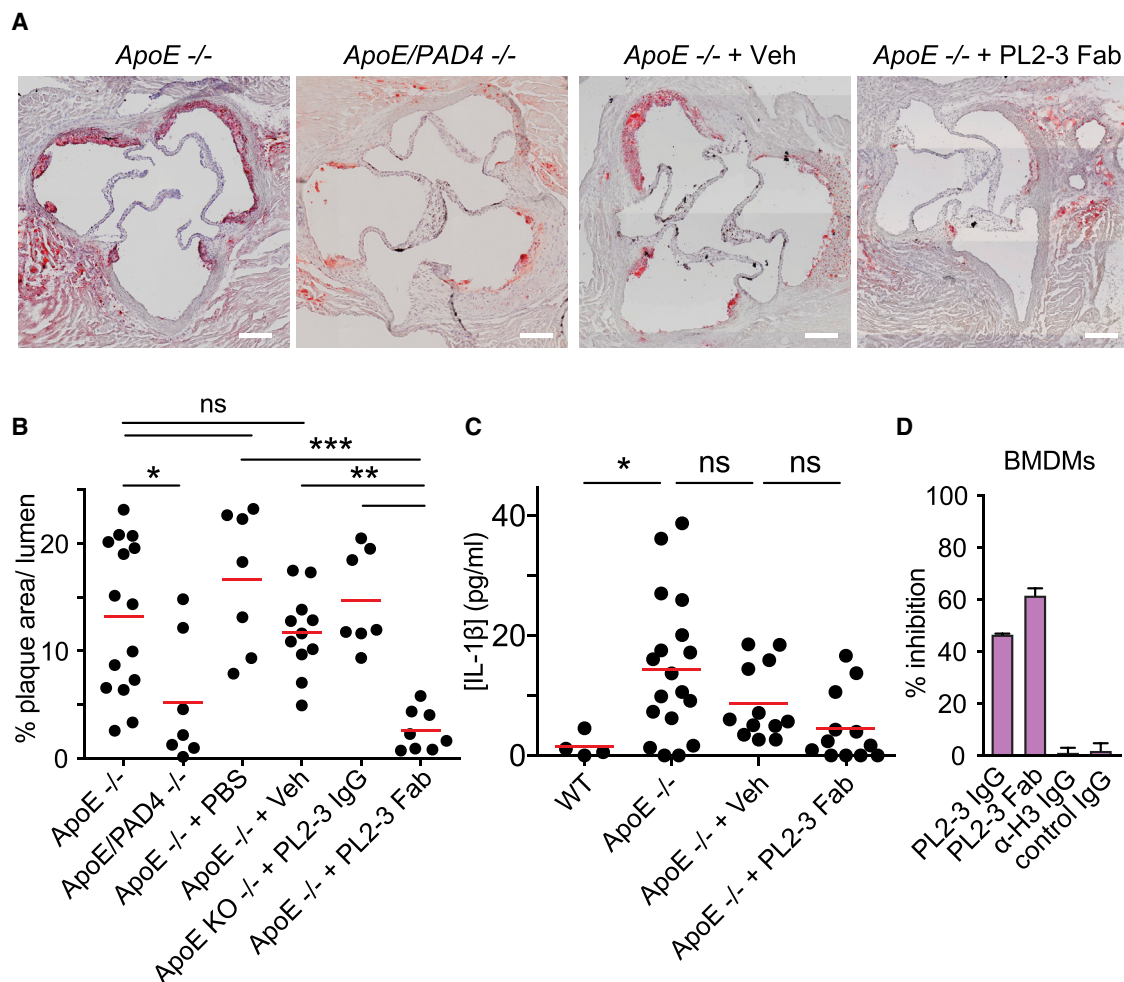


Figure 7. Citrullinated NET Chromatin Promotes Atherosclerosis

(A) Aortic root cross-sections from female ApoE-deficient or ApoE/PAD4-deficient animals untreated or treated with vehicle (Veh, Fab elution buffer) or an anti-chromatin PL2-3 Fab for 6 weeks on a high-fat diet. Sections were stained with the lipid dye Oil Red O (red) and counterstained with hematoxylin (scale bars, 200 μ m). Images are representative of at least 7 animals per group.

(B) Quantifications of average plaque size from several sections plotted as a fraction of lumen area from female ApoE-deficient or ApoE/PAD4-deficient animals untreated or treated with PBS or vehicle (Veh, Fab elution buffer) or an anti-chromatin PL2-3 full-length IgG or PL2-3 Fab for 6 weeks on a high-fat diet. Each point represents one animal. Statistical analysis by one-way ANOVA followed by Turkey's multiple comparison test.

(C) Plasma concentrations of IL-1 β from mice in (A). WT mice fed on regular chow until the same age were used as baseline controls. Each point represents one animal. Statistical analysis by Mann-Whitney test.

(D) Inhibition of total IL-1 β induction in WT murine BMDMs stimulated with 10^{-8} M mono-nucleosomes in the presence of PL2-3 IgG or Fab, anti-histone H3 (α -H3 IgG), or a control IgG. Data are represented as mean \pm SD.

* $p \leq 0.05$; ** $p \leq 0.01$; *** $p \leq 0.001$; ns, $p > 0.05$.

nucleosomes, whereas enzymes that completely remove DNA, such as DNase I, suppress inflammation by disrupting the synergy between DNA and histones.

Histone modifications, such as citrullination, that are found extensively in NETs also regulate the pro-inflammatory capacity of histones. Prior work has implicated PAD4 in atherosclerosis, suggesting that the decrease in the phenotype was associated with a defect in NET formation (Knight et al., 2014; Liu et al., 2018). Another study reported no differences in plaque size between chimeric mice receiving WT control cells and mice receiving PAD4-deficient cells and concluded that NETs were

not implicated in atherosclerotic lesion growth but affected fibrous cap thickness (Franck et al., 2018). Our experiments suggest that NETs still form in the plaques of PAD4-deficient animals but that citrullination enhances atherogenesis by potentiating the pro-inflammatory activity of histones. Compared to the more efficient plaque growth suppression by histone targeting or neutrophil protease deficiency (Warnatsch et al., 2015), the intermediate PAD4 deficient phenotype is consistent with a role for PAD4 in potentiating NET function rather than an absolute requirement for NET formation. Therefore, our observations support a role for PAD4 in atherogenesis but lead to a

reinterpretation of the mechanistic basis for PAD4-dependent phenotypes. Citrullination enhanced the binding of nucleosomes to TLR4, which provides a new mechanistic paradigm for citrullination and potentially other histone modifications in regulating the pro-inflammatory properties of NETs.

Our atherosclerosis and infection experiments now implicate chromatin histones not only as cytotoxic agents but also as signaling mediators that enhance inflammation during infection and sterile disease. Chromatin sensing might play beneficial or detrimental roles in potentiating inflammation during infection, depending on the context. The beneficial effects of DNase administration during infection argue toward a detrimental contribution of NET histones in hyperinflammatory scenarios (Pillai et al., 2016). Furthermore, uninfected mice tolerated the administration of the anti-chromatin PL2-3 Fab for several weeks. In contrast to animals deficient in neutrophil proteases that are known to affect inflammation in adipose tissues and elsewhere (Talukdar et al., 2012), we did not observe a statistically significant decrease in circulating cytokines as a result of PL2-3 Fab administration, whose effects were more localized, suggesting that systemic cytokines play a less important role in early atherogenesis. While the long-term effects of nucleosome targeting are unknown, targeting chromatin may provide a therapeutic avenue to treat chronic inflammatory diseases and acute inflammation by reducing pathogenic levels of cytokines without interfering with cytokine induction in response to microbial triggers.

STAR★METHODS

Detailed methods are provided in the online version of this paper and include the following:

- **KEY RESOURCES TABLE**
- **LEAD CONTACT AND MATERIALS AVAILABILITY**
 - Lead contact
 - Materials availability
 - Data and Code Availability
- **EXPERIMENTAL MODEL AND SUBJECT DETAILS**
 - Mice
 - Human blood samples
 - Human cell lines
- **METHOD DETAILS**
 - Cholesterol crystal preparation
 - Neutrophil isolation, NET imaging and preparation
 - Nucleosome isolation
 - Generation of recombinant MBP-Histone H3 and hPAD4 enzyme
 - Analysis of cytokine expression in human monocytes
 - Analysis of cytokine expression in BMDMs
 - Immunoprecipitation
 - Western blot analysis
 - TLR reporter line assay
 - Mice and atherosclerosis model
 - Flow cytometry
 - Immunofluorescence microscopy studies of TLR4 localization
- **QUANTIFICATION AND STATISTICAL ANALYSIS**

SUPPLEMENTAL INFORMATION

Supplemental Information can be found online at <https://doi.org/10.1016/j.celrep.2020.107602>.

ACKNOWLEDGMENTS

We thank Qingbo Xu for providing the ApoE-deficient mice, Kerri Mowen for the PAD4-deficient mice, and Marc Monestier for the PL2-3 anti-chromatin antibody. This work was supported by the Francis Crick Institute, which receives its core funding from the UK Medical Research Council (FC0010129), Cancer Research UK (FC0010129), and the Wellcome Trust (FC0010129).

AUTHOR CONTRIBUTIONS

T.-D.T. designed and performed the majority of the experiments. M.I. designed plasmids, generated recombinant protein, and performed flow cytometry. A.W., D.H., and Q.W. contributed to experiments. V.P. conceived and supervised the study. V.P. and T.-D.T. wrote the manuscript.

DECLARATIONS OF INTEREST

The authors declare no competing interests.

Received: March 15, 2019

Revised: December 13, 2019

Accepted: April 10, 2020

Published: May 5, 2020

REFERENCES

- Abrams, S.T., Zhang, N., Manson, J., Liu, T., Dart, C., Baluwa, F., Wang, S.S., Brohi, K., Kipar, A., Yu, W., et al. (2013). Circulating histones are mediators of trauma-associated lung injury. *Am. J. Respir. Crit. Care Med.* *187*, 160–169.
- Aga, E., Katschinski, D.M., van Zandbergen, G., Laufs, H., Hansen, B., Müller, K., Solbach, W., and Laskay, T. (2002). Inhibition of the spontaneous apoptosis of neutrophil granulocytes by the intracellular parasite *Leishmania major*. *J. Immunol.* *169*, 898–905.
- Atianand, M.K., and Fitzgerald, K.A. (2013). Molecular basis of DNA recognition in the immune system. *J. Immunol.* *190*, 1911–1918.
- Bertheloot, D., Naumovski, A.L., Langhoff, P., Horvath, G.L., Jin, T., Xiao, T.S., Garbi, N., Agrawal, S., Kolbeck, R., and Latz, E. (2016). RAGE Enhances TLR Responses through Binding and Internalization of RNA. *J. Immunol.* *197*, 4118–4126.
- Branzk, N., Lubojemska, A., Hardison, S.E., Wang, Q., Gutierrez, M.G., Brown, G.D., and Papayannopoulos, V. (2014). Neutrophils sense microbe size and selectively release neutrophil extracellular traps in response to large pathogens. *Nat. Immunol.* *15*, 1017–1025.
- Chamilos, G., Gregorio, J., Meller, S., Lande, R., Kontoyiannis, D.P., Modlin, R.L., and Gilliet, M. (2012). Cytosolic sensing of extracellular self-DNA transported into monocytes by the antimicrobial peptide LL37. *Blood* *120*, 3699–3707.
- Claushuis, T.A.M., van der Donk, L.E.H., Luitse, A.L., van Veen, H.A., van der Wel, N.N., van Vught, L.A., Roelofs, J.J.T.H., de Boer, O.J., Lankelma, J.M., Boon, L., et al. (2018). Role of Peptidylarginine Deiminase 4 in Neutrophil Extracellular Trap Formation and Host Defense during *Klebsiella pneumoniae*-Induced Pneumonia-Derived Sepsis. *J. Immunol.* *201*, 1241–1252.
- De Nardo, D., De Nardo, C.M., Nguyen, T., Hamilton, J.A., and Scholz, G.M. (2009). Signaling crosstalk during sequential TLR4 and TLR9 activation amplifies the inflammatory response of mouse macrophages. *J. Immunol.* *183*, 8110–8118.
- Fernandes-Alnemri, T., Yu, J.W., Datta, P., Wu, J., and Alnemri, E.S. (2009). AIM2 activates the inflammasome and cell death in response to cytoplasmic DNA. *Nature* *458*, 509–513.

- Franck, G., Mawson, T.L., Folco, E.J., Molinaro, R., Ruvkun, V., Engelbertsen, D., Liu, X., Tesmenitsky, Y., Shvartz, E., Sukhova, G.K., et al. (2018). Roles of PAD4 and NETosis in Experimental Atherosclerosis and Arterial Injury: Implications for Superficial Erosion. *Circ. Res.* **123**, 33–42.
- Gaidt, M.M., Ebert, T.S., Chauhan, D., Ramshorn, K., Pinci, F., Zuber, S., O'Duill, F., Schmid-Burgk, J.L., Hoss, F., Buhmann, R., et al. (2017). The DNA Inflammasome in Human Myeloid Cells Is Initiated by a STING-Cell Death Program Upstream of NLRP3. *Cell* **171**, 1110–1124.e18.
- Gehrke, N., Mertens, C., Zillinger, T., Wenzel, J., Bald, T., Zahn, S., Tüting, T., Hartmann, G., and Barchet, W. (2013). Oxidative damage of DNA confers resistance to cytosolic nuclease TREX1 degradation and potentiates STING-dependent immune sensing. *Immunity* **39**, 482–495.
- Hadjantonakis, A.K., and Papaioannou, V.E. (2004). Dynamic in vivo imaging and cell tracking using a histone fluorescent protein fusion in mice. *BMC Biotechnol.* **4**, 33.
- Hemmers, S., Tejaro, J.R., Arandjelovic, S., and Mowen, K.A. (2011). PAD4-mediated neutrophil extracellular trap formation is not required for immunity against influenza infection. *PLoS ONE* **6**, e22043.
- Hemmi, H., Takeuchi, O., Kawai, T., Kaisho, T., Sato, S., Sanjo, H., Matsumoto, M., Hoshino, K., Wagner, H., Takeda, K., and Akira, S. (2000). A Toll-like receptor recognizes bacterial DNA. *Nature* **408**, 740–745.
- Hornung, V., Ablasser, A., Charrel-Dennis, M., Bauernfeind, F., Horvath, G., Caffrey, D.R., Latz, E., and Fitzgerald, K.A. (2009). AIM2 recognizes cytosolic dsDNA and forms a caspase-1-activating inflammasome with ASC. *Nature* **458**, 514–518.
- Hoshino, K., Takeuchi, O., Kawai, T., Sanjo, H., Ogawa, T., Takeda, Y., Takeda, K., and Akira, S. (1999). Cutting edge: Toll-like receptor 4 (TLR4)-deficient mice are hyporesponsive to lipopolysaccharide: evidence for TLR4 as the Lps gene product. *J. Immunol.* **162**, 3749–3752.
- Huang, H., Evankovich, J., Yan, W., Nace, G., Zhang, L., Ross, M., Liao, X., Biliar, T., Xu, J., Esmon, C.T., and Tsung, A. (2011). Endogenous histones function as alarmins in sterile inflammatory liver injury through Toll-like receptor 9 in mice. *Hepatology* **54**, 999–1008.
- Ishikawa, H., and Barber, G.N. (2008). STING is an endoplasmic reticulum adaptor that facilitates innate immune signalling. *Nature* **455**, 674–678.
- Kenny, E.F., Herzig, A., Krüger, R., Muth, A., Mondal, S., Thompson, P.R., Brinkmann, V., Bernuth, H.V., and Zychlinsky, A. (2017). Diverse stimuli engage different neutrophil extracellular trap pathways. *eLife* **6**, e24437.
- Knight, J.S., Luo, W., O'Dell, A.A., Yalavarthi, S., Zhao, W., Subramanian, V., Guo, C., Grenn, R.C., Thompson, P.R., Eitzman, D.T., and Kaplan, M.J. (2014). Peptidylarginine deiminase inhibition reduces vascular damage and modulates innate immune responses in murine models of atherosclerosis. *Circ. Res.* **114**, 947–956.
- Kumar, S.V., Kulkarni, O.P., Mulay, S.R., Darisipudi, M.N., Romoli, S., Thomasova, D., Scherbaum, C.R., Hohenstein, B., Hugo, C., Müller, S., et al. (2015). Neutrophil Extracellular Trap-Related Extracellular Histones Cause Vascular Necrosis in Severe GN. *J. Am. Soc. Nephrol.* **26**, 2399–2413.
- Lande, R., Gregorio, J., Facchinetti, V., Chatterjee, B., Wang, Y.H., Homey, B., Cao, W., Wang, Y.H., Su, B., Nestle, F.O., et al. (2007). Plasmacytoid dendritic cells sense self-DNA coupled with antimicrobial peptide. *Nature* **449**, 564–569.
- Lande, R., Ganguly, D., Facchinetti, V., Frasca, L., Conrad, C., Gregorio, J., Meller, S., Chamilos, G., Sebasigari, R., Ricci, V., et al. (2011). Neutrophils activate plasmacytoid dendritic cells by releasing self-DNA-peptide complexes in systemic lupus erythematosus. *Sci. Transl. Med.* **3**, 73ra19.
- Leppkes, M., Maueröder, C., Hirth, S., Nowecki, S., Günther, C., Billmeier, U., Paulus, S., Biermann, M., Munoz, L.E., Hoffmann, M., et al. (2016). Externalized decondensed neutrophil chromatin occludes pancreatic ducts and drives pancreatitis. *Nat. Commun.* **7**, 10973.
- Leshner, M., Wang, S., Lewis, C., Zheng, H., Chen, X.A., Santy, L., and Wang, Y. (2012). PAD4 mediated histone hypercitrullination induces heterochromatin decondensation and chromatin unfolding to form neutrophil extracellular trap-like structures. *Front. Immunol.* **3**, 307.
- Liu, Y., Carmona-Rivera, C., Moore, E., Seto, N.L., Knight, J.S., Pryor, M., Yang, Z.H., Hemmers, S., Remaley, A.T., Mowen, K.A., and Kaplan, M.J. (2018). Myeloid-Specific Deletion of Peptidylarginine Deiminase 4 Mitigates Atherosclerosis. *Front. Immunol.* **9**, 1680.
- Lood, C., Blanco, L.P., Purmalek, M.M., Carmona-Rivera, C., De Ravin, S.S., Smith, C.K., Malech, H.L., Ledbetter, J.A., Elkon, K.B., and Kaplan, M.J. (2016). Neutrophil extracellular traps enriched in oxidized mitochondrial DNA are interferogenic and contribute to lupus-like disease. *Nat. Med.* **22**, 146–153.
- Losman, M.J., Fasy, T.M., Novick, K.E., and Monestier, M. (1992). Monoclonal autoantibodies to subnucleosomes from a MRL/Mp(-)/+ mouse. Oligoclonality of the antibody response and recognition of a determinant composed of histones H2A, H2B, and DNA. *J. Immunol.* **148**, 1561–1569.
- Muñoz, L.E., Bilyy, R., Biermann, M.H., Kienhöfer, D., Maueröder, C., Hahn, J., Brauner, J.M., Weidner, D., Chen, J., Scharin-Mehlmann, M., et al. (2016). Nanoparticles size-dependently initiate self-limiting NETosis-driven inflammation. *Proc. Natl. Acad. Sci. USA* **113**, E5856–E5865.
- Napolitani, G., Rinaldi, A., Bertoni, F., Sallusto, F., and Lanzavecchia, A. (2005). Selected Toll-like receptor agonist combinations synergistically trigger a T helper type 1-polarizing program in dendritic cells. *Nat. Immunol.* **6**, 769–776.
- Negishi, H., Yanai, H., Nakajima, A., Koshiba, R., Atarashi, K., Matsuda, A., Matsuki, K., Miki, S., Doi, T., Aderem, A., et al. (2012). Cross-interference of RLR and TLR signaling pathways modulates antibacterial T cell responses. *Nat. Immunol.* **13**, 659–666.
- Paludan, S.R., and Bowie, A.G. (2013). Immune sensing of DNA. *Immunity* **38**, 870–880.
- Papayannopoulos, V., Metzler, K.D., Hakkim, A., and Zychlinsky, A. (2010). Neutrophil elastase and myeloperoxidase regulate the formation of neutrophil extracellular traps. *J. Cell Biol.* **191**, 677–691.
- Piedrahita, J.A., Zhang, S.H., Hagaman, J.R., Oliver, P.M., and Maeda, N. (1992). Generation of mice carrying a mutant apolipoprotein E gene inactivated by gene targeting in embryonic stem cells. *Proc. Natl. Acad. Sci. USA* **89**, 4471–4475.
- Pillai, P.S., Molony, R.D., Martinod, K., Dong, H., Pang, I.K., Tal, M.C., Solis, A.G., Bielecki, P., Mohanty, S., Trentalange, M., et al. (2016). Mx1 reveals innate pathways to antiviral resistance and lethal influenza disease. *Science* **352**, 463–466.
- Schauer, C., Janko, C., Munoz, L.E., Zhao, Y., Kienhöfer, D., Frey, B., Lell, M., Manger, B., Rech, J., Naschberger, E., et al. (2014). Aggregated neutrophil extracellular traps limit inflammation by degrading cytokines and chemokines. *Nat. Med.* **20**, 511–517.
- Silvestre-Roig, C., Braster, Q., Wichapong, K., Lee, E.Y., Teulon, J.M., Berrebeh, N., Winter, J., Adrover, J.M., Santos, G.S., Froese, A., et al. (2019). Externalized histone H4 orchestrates chronic inflammation by inducing lytic cell death. *Nature* **569**, 236–240.
- Sirois, C.M., Jin, T., Miller, A.L., Bertheloot, D., Nakamura, H., Horvath, G.L., Mian, A., Jiang, J., Schrum, J., Bossaller, L., et al. (2013). RAGE is a nucleic acid receptor that promotes inflammatory responses to DNA. *J. Exp. Med.* **210**, 2447–2463.
- Sun, L., Wu, J., Du, F., Chen, X., and Chen, Z.J. (2013). Cyclic GMP-AMP synthase is a cytosolic DNA sensor that activates the type I interferon pathway. *Science* **339**, 786–791.
- Talukdar, S., Oh, D.Y., Bandyopadhyay, G., Li, D., Xu, J., McNelis, J., Lu, M., Li, P., Yan, Q., Zhu, Y., et al. (2012). Neutrophils mediate insulin resistance in mice fed a high-fat diet through secreted elastase. *Nat. Med.* **18**, 1407–1412.
- Tan, R.S., Ho, B., Leung, B.P., and Ding, J.L. (2014). TLR cross-talk confers specificity to innate immunity. *Int. Rev. Immunol.* **33**, 443–453.
- Tian, J., Avalos, A.M., Mao, S.Y., Chen, B., Senthil, K., Wu, H., Parroche, P., Drabic, S., Golenbock, D., Sirois, C., et al. (2007). Toll-like receptor 9-dependent activation by DNA-containing immune complexes is mediated by HMGB1 and RAGE. *Nat. Immunol.* **8**, 487–496.
- Ulas, T., Pirr, S., Fehlhaber, B., Bickes, M.S., Loof, T.G., Vogl, T., Mellinger, L., Heinemann, A.S., Burgmann, J., Schöning, J., et al. (2017). S100-alarmin-

induced innate immune programming protects newborn infants from sepsis. *Nat. Immunol.* **18**, 622–632.

Urban, C.F., Ermert, D., Schmid, M., Abu-Abed, U., Goosmann, C., Nacken, W., Brinkmann, V., Jungblut, P.R., and Zychlinsky, A. (2009). Neutrophil extracellular traps contain calprotectin, a cytosolic protein complex involved in host defense against *Candida albicans*. *PLoS Pathog.* **5**, e1000639.

Urbonaviciute, V., Fürrohr, B.G., Meister, S., Munoz, L., Heyder, P., De Marchis, F., Bianchi, M.E., Kirschning, C., Wagner, H., Manfredi, A.A., et al. (2008). Induction of inflammatory and immune responses by HMGB1-nucleosome complexes: implications for the pathogenesis of SLE. *J. Exp. Med.* **205**, 3007–3018.

Vogl, T., Tenbrock, K., Ludwig, S., Leukert, N., Ehrhardt, C., van Zoelen, M.A., Nacken, W., Foell, D., van der Poll, T., Sorg, C., and Roth, J. (2007). Mrp8 and Mrp14 are endogenous activators of Toll-like receptor 4, promoting lethal, endotoxin-induced shock. *Nat. Med.* **13**, 1042–1049.

Wang, Y., Li, M., Stadler, S., Correll, S., Li, P., Wang, D., Hayama, R., Leonelli, L., Han, H., Grigoryev, S.A., et al. (2009). Histone hypercitrullination mediates

chromatin decondensation and neutrophil extracellular trap formation. *J. Cell Biol.* **184**, 205–213.

Warnatsch, A., Ioannou, M., Wang, Q., and Papayannopoulos, V. (2015). Inflammation. Neutrophil extracellular traps license macrophages for cytokine production in atherosclerosis. *Science* **349**, 316–320.

Westman, J., Papareddy, P., Dahlgren, M.W., Chakrakodi, B., Norrby-Te-glund, A., Smeds, E., Linder, A., Mörgelin, M., Johansson-Lindbom, B., Egesten, A., and Herwald, H. (2015). Extracellular Histones Induce Chemokine Production in Whole Blood Ex Vivo and Leukocyte Recruitment In Vivo. *PLoS Pathog.* **11**, e1005319.

Xu, J., Zhang, X., Pelayo, R., Monestier, M., Ammollo, C.T., Semeraro, F., Taylor, F.B., Esmon, N.L., Lupu, F., and Esmon, C.T. (2009). Extracellular histones are major mediators of death in sepsis. *Nat. Med.* **15**, 1318–1321.

Xu, J., Zhang, X., Monestier, M., Esmon, N.L., and Esmon, C.T. (2011). Extracellular histones are mediators of death through TLR2 and TLR4 in mouse fatal liver injury. *J. Immunol.* **187**, 2626–2631.

STAR★METHODS

KEY RESOURCES TABLE

REAGENT or RESOURCE	SOURCE	IDENTIFIER
Antibodies		
Anti-HA tag antibody	Abcam	Ab9110; RRID: AB_307019
Histone H3 (citrulline R2+R8+R17) (anti-cit-H3)	Abcam	Ab5103; RRID: AB_304752
Rabbit IgG, polyclonal - Isotype Control	Abcam	Ab37415; RRID: AB_2631996
TLR4 antibody	Abcam	Ab22048; RRID: AB_446735
Mouse IgG1 kappa isotype control antibody	Antibodies online	ABIN2704378; RRID: AB_2833099
S100A8 antibody	Antibodies online	ABIN111892; RRID: AB_2833100
PE Mouse Anti-Human TLR4 (CD284), Clone TF901	BD biosciences	564215; RRID: AB_2738674
Alexa Fluor 647-anti-mouse-Ly6G-antibody	Biolegend	127610; RRID: AB_1134159
Maltose Binding Protein (MBP) antibody	Biolegend	906901; RRID: AB_2565070
Rab5 antibody	Cell Signaling Technology	C8B1 - 3547; RRID: AB_2300649
Neutrophil elastase antibody	GeneTex	GTX2042; RRID: AB_383332
TLR2 neutralizing antibody	Invivogen	pab-hstlr2; RRID: AB_11124921
TLR4 neutralizing antibody	Invivogen	pab-hstlr4; RRID: AB_11125132
PL2-3 anti-chromatin mouse antibody	Losman et al., 1992	N/A
Histone H3 antibody	Millipore	07-690; RRID: AB_417398
Myeloperoxidase antibody	R&D	AF3667; RRID: AB_2250866
Chemicals, Peptides, and Recombinant Proteins		
AnyKD Criterion TGX Precast Midi Protein Gel	Bio-Rad Laboratories	5671124
Trans-Blot Turbo Midi PVDF membrane	Bio-Rad Laboratories	1704157
Histone H3 (human recombinant)	Cayman Chemical	10263
SYTOX green	Invitrogen	S7020
LPS-SM (LPS from <i>S. minnesota</i> R595)	Invivogen	tlrl-smllps
FSL-1	Invivogen	tlrl-fsl
CD14 microbeads	MACS Miltenyi	130-050-201
Chloride-amidine	Merk Millipore	506282
BseRI	New England Biolabs	R0581S
Pacl	New England Biolabs	R0547S
NdeI	New England Biolabs	R0111S
AflII	New England Biolabs	R0541S
Amylose Resin high flow	New England Biolabs	E8022S
Micrococcal Nuclease (MNase)	New England Biolabs	M0247S
Cholesterol	Sigma	C8667
cOmplete, Mini, EDTA-free Protease Inhibitor Cocktail	Sigma-Aldrich	4693159001
Bafilomycin A1 from <i>Streptomyces griseus</i>	Sigma-Aldrich	B1793
Benzonase® Nuclease	Sigma-Aldrich	E1014
ProLong Gold Antifade Mountant	ThermoFisher scientific	P36930
DAPI(4',6-Diamidino-2-Phenylindole, Dihydrochloride)	ThermoFisher scientific	D1306
LIVE/DEAD Fixable Blue Dead Cell Stain Kit	ThermoFisher scientific	L34961
Critical Commercial Assays		
Human IFN-beta ELISA Kit	R&D systems	41410-1
Limulus amoebocyte lysate assay	ThermoFisher scientific	88282
Pierce Fab Preparation Kit	ThermoFisher scientific	44985

(Continued on next page)

Continued		
REAGENT or RESOURCE	SOURCE	IDENTIFIER
IL-1 beta Human Uncoated ELISA Kit	ThermoFisher scientific	88-7261-77
IL-1 beta Mouse Uncoated ELISA Kit	ThermoFisher scientific	88-7013-88
Interferon alpha (Cell culture) Human ELISA Kit	ThermoFisher scientific	411001
IFN-alpha/IFN-beta 2-Plex Mouse ProcartaPlex Panel	ThermoFisher scientific	EPX02A-22187-901
Experimental Models: Cell Lines		
Human HL-60 HL-60 (ATCC® CCL-240)	ATCC	CCL-240
HEK-Blue hTLR2	Invivogen	hkb-hltr2
HEK-Blue hTLR4	Invivogen	hkb-hltr4
HEK-Blue hTLR9	Invivogen	hkb-hltr9
HEK-Blue Null1 Cells	Invivogen	hkb-null1
HEK-Blue Null2 Cells	Invivogen	hkb-null2
293/hTLR2-HA	Invivogen	293-hltr2ha
293/hTLR4-HA	Invivogen	293-hltr4ha
293/Null	Invivogen	293-null
Experimental Models: Organisms/Strains		
WT <i>C. albicans</i> SC5314	Arturo Zychlinsky	N/A
TLR9 $-/-$ (C57BL/6J- <i>Tlr9</i> ^{M7Btr} /Mmjax)	Hemmi et al., 2000	N/A
TLR4 $-/-$ (B6(Cg)- <i>Tlr4</i> ^{tm1.2Karp} /J)	Hoshino et al., 1999	N/A
STING $-/-$ (B6(Cg)- <i>Sting</i> ^{tm1.2Camb} /J)	Ishikawa and Barber, 2008	N/A
ApoE $-/-$ (B6.129P2-ApoE ^{tm1Unc} /J)	Piedrahita et al., 1992	N/A
ApoE/PAD4 $-/-$	This paper	N/A
PAD4 $-/-$ (B6.Cg-Padi4 ^{tm1.1Krow} /J)	Hemmers et al., 2011	N/A
CAG::H2-EGFP (B6.Cg-Tg(HIST1H2BB/EGFP)1Pa/J)	The Jackson Laboratory	006069; RRID: IMSR_JAX:006069
Oligonucleotides		
human ODN 2006 (ODN 7909)	Invivogen	tlr1-2006
BamHI-H3.1-Forward primer: 5-CGCGGATCCATGGCTC GTACTAAGCAG-3	Sigma-Aldrich	N/A
BamHI-hPAD4-forward: 5-CACGGATCCATGGCCCAG GGGACATTG-3	Sigma-Aldrich	N/A
Sall-hPAD4-Reverse: 5-GCGGTCGACTCAGGGCACC ATGTTCC-3	Sigma-Aldrich	N/A
XhoI-H3.1-Reverse primer: 5-GAGCTCGAGTTACGCCC TCTCCCCGC-3	Sigma-Aldrich	N/A
TaqMan® Gene Expression Assay, Assay ID: Hs00174092_m1, human IL1A	ThermoFisher scientific	4331182
TaqMan® Gene Expression Assay, Assay ID: Hs00174131_m1, human IL6	ThermoFisher scientific	4331182
TaqMan® Gene Expression Assay, Human HPRT1 Hs02800695_m1	ThermoFisher scientific	4331182
TaqMan® Gene Expression Assay, human IL1B Hs01555410_m1	ThermoFisher scientific	4331182
Recombinant DNA		
pMAL-c2X plasmid	Addgene	75286
Software and Algorithms		
Fiji/ImageJ version 2.0.0	https://imagej.net/Contributors	https://imagej.net/Fiji
FlowJo version 10	Becton Dickinson	https://www.flowjo.com
GraphPad Prism Version 7	GraphPad Inc.	https://www.graphpad.com/scientific-software/prism/
Other		
L929 cell culture supernatant	The Francis Crick Institute – Cell services core facility	N/A

LEAD CONTACT AND MATERIALS AVAILABILITY

Lead contact

This study did not generate new unique reagents. Further information should be requested by the Lead Contact, Venizelos Papayannopoulos (veni.p@crick.ac.uk).

Materials availability

Requests for resources and reagents should be directed to and will be fulfilled by the Lead Contact, Venizelos Papayannopoulos (veni.p@crick.ac.uk).

Data and Code Availability

This study did not generate or analyze datasets or code.

EXPERIMENTAL MODEL AND SUBJECT DETAILS

Mice

All mice were bred and maintained on a C57BL/6J background in a pathogen free, 12-hour light-dark cycle environment. All experiments were performed under an approved project license and following the UK Home Office regulations under the Animals Scientific Procedures Act 1986 (ASPA). ApoE/PAD4 deficient mice were generated by crossing ApoE deficient ([Piedrahita et al., 1992](#)) on a C57BL/6J background with PAD4 deficient mice ([Hemmers et al., 2011](#)) on a C57BL/6J background for at least 10 generations. 8-10 week old female mice were used in all experiments unless otherwise specified.

Human blood samples

Peripheral blood was isolated from consenting healthy adult volunteers, according to approved protocols of the ethics board of the Francis Crick Institute and the Tissue act.

Human cell lines

HL-60 is an acute promyelocytic leukemia cell line isolated from a 36-year-old Caucasian female. The cells were expanded in suspension in IMDM supplemented with 10% heat-inactivated fetal calf serum (Gibco), 100U/ml penicillin and 100μg/ml streptomycin. HEK-Blue TLR cells (Invivogen) are human embryonic kidney 293 (HEK293) engineered cell lines that stably co-express the relevant TLR gene and an inducible SEAP (secreted embryonic alkaline phosphatase) reporter gene. Cells along with their parental lines were maintained in DMEM supplemented with 4.5g/L glucose and 2mM L-glutamine, 10% heat-inactivated fetal calf serum (GIBCO), 100U/ml penicillin, 100μg/ml streptomycin, 100μg/ml Normocin (Invivogen) and the relevant selection antibiotic as per manufacturer instructions (Invivogen). 293/TLR-HA cells are generated by stable transfection of the HEK293 cell line with the TLR gene fused to the influenza hemagglutinine (HA) tag. Cells along with their parental lines were maintained in DMEM supplemented with 4.5g/L glucose and 2mM L-glutamine, 10% heat-inactivated fetal calf serum (GIBCO), 50U/ml penicillin, 50μg/ml streptomycin, 100μg/ml Normocin (Invivogen) and 10μg/ml blasticidin as per manufacturer instructions (Invivogen). All cell lines were maintained in a 5% CO₂ humidified incubator at 37°C.

METHOD DETAILS

Cholesterol crystal preparation

Cholesterol (Sigma-Aldrich) was solubilized in 95% Ethanol by incubating at 65°C, at a concentration of 12.5mg/ml. Cholesterol crystals were formed by 5 consecutive freezing/thawing cycles., spun down at 13000rpm and resuspended in phosphate-buffered saline (PBS, GIBCO), at a concentration of 5mg/ml. Reagents were sterile and endotoxin-free, as confirmed by Limulus amoebocyte lysate assay (Thermo fisher scientific).

Neutrophil isolation, NET imaging and preparation

Neutrophils were isolated with a two-step purification protocol using histopaque separation followed by a discontinuous Percoll gradient ([Aga et al., 2002](#)). Isolated neutrophils were plated in the presence or absence of 200 μM PAD inhibitor Chloride-amidine (Cl⁻ amidine) (Merk Millipore). After 30 min settling, the neutrophils were stimulated with 0.5mg/ml cholesterol crystals. After 4 hours of incubation at 37°C, NET formation was confirmed by visualization using 0.1 μM SYTOX green (Invitrogen) and images were captured using a LEICA DMIRB microscope (20x objective) and analyzed using Fiji/ImageJ software. NET release was quantitated using ImageJ software as previously described ([Papayannopoulos et al., 2010](#)) and results were plotted using the frequency function in Microsoft Excel as the area of distribution of SYTOX⁺ events relative to total cells counted by phase-contrast microscopy. For immunofluorescence analysis of NETs, four hours after cholesterol crystal stimulation, cells were fixed for 20 min at RT with 2% paraformaldehyde and permeabilized with 0.5% Triton X-100 in PBS. Subsequently, samples were blocked with 2% bovine serum albumin (BSA) and 2% donkey serum in phosphate-buffered saline and incubated with anti-histone 3 citrulline R2+R8+R17 (Abcam),

anti-human neutrophil elastase (GeneTex) and anti-human myeloperoxidase (R&D) antibodies, followed by Alexa Fluor 488–conjugated donkey anti-goat, Alexa Fluor 568–conjugated donkey anti-rabbit and Alexa Fluor 647–conjugated donkey anti-mouse (all by Invitrogen). Samples were counterstained with DAPI (4',6-diamidino-2-phenylindole dihydrochloride; ThermoFisher Scientific) before being mounted in ProLong Gold (ThermoFisher Scientific) and examined by confocal microscopy. Images were analyzed with ImageJ v2.0 software. For NET preparations, after overnight incubation with cholesterol crystal stimulation, the culture medium was removed and a restriction enzyme mix containing BseRI, PaeI, NdeI and AflIII (5U/ml in Cut Smart NEB buffer, New England Biolabs) was added and incubated at 37°C for 30–60 min to achieve partial NET digestion. NET DNA concentration was determined using Quant-iT PicoGreen dsDNA Reagent (Thermo Fisher Scientific) after a Proteinase K (New England Biolabs) treatment (100U/ml for 2 hours at 56°C). Equal amounts of NETs containing 120ng of DNA were analyzed by Western-blot using anti-histone H3 citrulline R2+R8+R17 (Abcam), anti-human histone H3 (Millipore) anti-human myeloperoxidase (R&D) and anti-human S100A8 (antibodies online).

Nucleosome isolation

HL-60 cells or cells from homogenized lung, liver and spleen of WT or CAG::H2B-EGFP transgenic mice (Hadjantonakis and Papaioannou, 2004), were lysed on ice in a buffer containing 20mM HEPES pH7.5, 0.25M Sucrose, 3mM MgCl₂, 20mM KCl, 0.1% NP-40, 1mM DTT, 0.4mM PMSF and 1x cOmplete protease inhibitor cocktail tablet (Sigma-Aldrich). The lysate was then layered over equal volume of lysis buffer containing 2M sucrose and spun at 800 g for 20 min. Pelleted nuclei were resuspended in 20mM HEPES pH7.5, 3mM MgCl₂, 0.2mM EGTA, 1mM DTT, 0.4mM PMSF and 1x cOmplete protease inhibitor cocktail tablet. An equal volume of the same buffer supplemented with 0.6M KCl and 10% glycerol was added over gentle vortex. After a short incubation on ice, the preparation was pelleted at 17500 g. The pellet was resuspended using a douncer in 20mM HEPES pH7.5, 0.4M NaCl, 1mM EDTA, 5% glycerol, 1mM DTT, 0.5mM PMSF and 1x cOmplete. After centrifugation at 10000 g, pellets were resuspended in a high salt buffer containing 20mM HEPES pH7.5, 0.65M NaCl, 1mM EDTA, 0.34M sucrose, 1mM DTT, 0.5mM PMSF and 1x cOmplete, and were homogenized using a tight dounce for 40–50 strokes. After a final centrifugation at 10000 g to remove any unopened nuclei and nuclear debris, the supernatant was dialyzed overnight into a low salt buffer of 20mM HEPES pH7.5, 0.1M NaCl, 1mM EDTA, 1mM DTT and 0.5mM PMSF, using a 2kDa dialysis cassette (Thermo Fisher Scientific). To digest the nucleosome preparations, a final concentration of 3mM CaCl₂ was added for digestion with 10U/ml micrococcal nuclease (MNase, New England Biolabs) or 2mM MgCl for the digestion with 50U/ml Benzonase or 20U/ml DNase I (both Sigma-Aldrich). DNA amounts and fragment size were assessed by electrophoresis after Proteinase K treatment on a small sample at a 1% agarose gel. Nucleosomal DNA digestions were terminated by Ca²⁺ chelation with 50mM EGTA and the salt concentration was increased to 0.65M NaCl. To prepare Proteinase K-digested nucleosomes, after MNase digestion to a 0.2kb DNA length, preps were incubated with proteinase K and then heat-inactivated at 99°C. Lack of intact proteins was confirmed by electrophoresis and InstantBlue Coomassie Stain (Expedeon Protein Solutions). EGTA was dialyzed away using a 2kDa dialysis cassette and any aggregates were removed with high speed centrifugation before use.

Generation of recombinant MBP-Histone H3 and hPAD4 enzyme

Histone H3.1 was amplified from a cDNA library derived from mouse splenocytes using a BamHI-H3.1-Forward primer: 5-CGCGGATCCATGGCTCGTACTAAGCAG-3 and an XhoI-H3.1-Reverse primer: 5-GAGCTCGAGTTACGCCCTCTCCCCGC-3. The PCR fragment was digested and gel purified, then ligated to a pMAL-c2x plasmid cleaved with BamHI and Sall (New England Biolabs). A TEV protease cleavage sequence was introduced preceding the H3.1 using BclI (New England Biolabs) and BamHI. MBP-FXa-TEV-H3.1 (described as MBP-H3) or MBP-FXa (described as MBP). Constructs were expressed in BL21(DE3) *E. coli* cells. Cultures were grown in Lysogeny broth (LB) medium at 37°C. Expression was induced at OD₆₀₀ = 0.4 with 200 μM IPTG and cells were incubated at 37°C for 3h. MBP-H3 and MBP were purified in 20mM Tris pH7.4, 200mM NaCl and 1mM DTT using Amylose Resin high flow (New England Biolabs). Protein elution was achieved by adding 10mM Maltose (Sigma-Aldrich). hPAD4 was amplified from a cDNA library of human neutrophils using the primers BamHI-hPAD4-forward: 5-CACGGATCCATGGCCCAGGGGACATTG-3 and Sall-hPAD4-Reverse: 5-GCGGTCTGACTCAGGGCACCATGTTCC-3 and subsequently cleaved with BamHI/Sall (New England Biolabs). hPAD4 was then ligated to a pET vector (pBH8) backbone, containing a 6His-tag on the N-terminal site, previously linearized with BamHI and Sall. 6His-hPAD4 was amplified in DH5α *E. coli* then recombinantly expressed in BL21(DE3) *E. coli* cells. Cultures were grown in Lysogeny broth (LB) medium at 37°C. Protein expression was induced at OD₆₀₀ = 0.4 with 200 μM IPTG and cells were incubated at 25°C for 5h. 6His-hPAD4 was purified in 20mM Tris pH8, 300mM NaCl and 10mM Imidazole using Ni-NTA beads. Protein was eluted with 250mM Imidazole, dialyzed in 20mM Tris pH8, 200mM NaCl, 1mM DTT and 2mM CaCl₂. Ion exchange chromatography was performed using a Q-Sepharose column (Resource™ Q, GE lifesciences, 1ml) and the sample was eluted with a 200 μM–1M NaCl gradient. The fractions containing the enzyme were identified by tandem mass spectrometry and enzymatic activity was confirmed on recombinant histones (Cayman).

Analysis of cytokine expression in human monocytes

Peripheral blood mononuclear cells (PBMCs) were isolated from consenting healthy adult volunteers by centrifugation over a Histopaque-1119 gradient (Sigma-Aldrich). CD14-positive monocytes were isolated using MACS CD14 microbeads (MACS Miltenyi Biotec) according to manufacturer instructions. Cells were plated in HBSS with Ca²⁺ and Mg²⁺ supplemented with 10% heat-inactivated

fetal calf serum (GIBCO). In some cases, cells were preincubated with 5ug/ml anti-TLR2 and anti-TLR4 neutralizing antibodies (Invivogen, pab-hstlr2 and pab-hstlr4) or 50nM Bafilomycin A1 (Sigma-Aldrich) before being stimulated with the indicated concentrations of NET fragments preparations (500ng/ml as per DNA content, with or without pretreatment with 20U/ml DNase I for 2 hours), Nucleosome preparations (prepared from either HL-60 or H2B-EGFP cells), recombinant human Histone H3 (Cayman), recombinant human Histone H3 citrullinated overnight at 37°C with PAD4 (100μM Histone-3 with 25nM recombinant human PAD4) preincubated with NET DNA (purified from NET fragment preparations cleaned of protein content, using the QIAquick Gel extraction kit by QIAGEN following manufacturer's instructions), CpG ODN 2006 (Invivogen) or LPS from Salmonella Minnesota R595 (Invivogen). All stimulants except for LPS, were pretreated with 50ug/ml of Polymyxin B (Invivogen) to neutralise any potential endotoxin contamination. After overnight incubation, 0.1% NP-40 and 1x cComplete protease inhibitor tablet were added to the medium and the lysates were analyzed for human IL-1β, IFN-α and IFN-β via ELISA according to the manufacturer's instructions. For cytokine mRNA level assessment, monocytes were incubated with the indicated stimulants for 2 hours at 37°C. Total cellular RNA was isolated using the TriReagent/Chloroform/Isopropanol (Sigma-Aldrich) method. 2 μg of RNA were then used to perform reverse transcription and generate cDNA using the Transcriptor high fidelity cDNA synthesis kit from Roche using anchored-oligo(dT)18 primer. Gene expression was measured using TaqMan Universal PCR Master Mix with IL-1β, IL-1α, IL-6 and HPRT-1 specific primers on a 7900HT Fast Real Time PCR System (Applied biosystems). The cycling threshold for each cytokine was analyzed and then normalized to that of HPRT1. Then, the relative gene expression was measured by the change in cyclin threshold ($\Delta\Delta CT$) method.

Analysis of cytokine expression in BMDMs

Bone marrow was isolated from the femur and tibia from WT C57BL/6J mice or animals deficient in TLR4 or TLR9 or STING or CAG::H2B-EGFP transgenic animals (Hadjantonakis and Papaioannou, 2004; Hemmi et al., 2000; Hoshino et al., 1999; Ishikawa and Barber, 2008). Red blood cells were lysed using ACK lysis buffer (GIBCO) and the remaining cells were cultured in DMEM supplemented with 20% L929 cell culture supernatant (The Francis Crick Institute – cell services core facility), 10mM HEPES (Lonza), 1% L-glutamine (GIBCO), 10% FCS (Invitrogen), 100 U/ml penicillin and 100ug/ml streptomycin (GIBCO) and 0.05mM 2-mercaptoethanol (GIBCO) for 7 days. Cells were washed in PBS and collected using 2.5mM EDTA (Invitrogen) in PBS with 5% FCS. Cells were then cultured overnight in DMEM with 1% FCS, 1% L-glutamine, 100U/ml penicillin and 100ug/ml streptomycin, 10 μM HEPES and 0.05mM 2-mercaptoethanol. Cells were stimulated with the indicated concentrations of HL-60 nucleosome preparations, recombinant citrullinated histone H3 (Cayman) with DNA, CpG ODN2006(Invivogen) or LPS from Salmonella Minnesota R595 (Invivogen). All stimulants except for LPS, were pretreated with 50ug/ml of Polymyxin B (Invivogen) to neutralise any potential endotoxin contamination. 1% NP-40 and 1x cComplete was added to the medium and the lysates were analyzed for mouse IL-1β, IFN-α and IFN-β via ELISA (ThermoFisher Scientific) according to the manufacturer's instructions.

Immunoprecipitation

293 cell lines stably expressing the relevant TLR gene fused at the 3' end to the influenza hemagglutinine (HA) tag were obtained by Invivogen and cultured according to the manufacturer's instructions. 293/TLR2-HA and 293/TLR4-HA cells were stimulated for 2 hours with 1 μM MBP-H3 or 1 μM of MBP (preincubated with or without 80ng of NET DNA), 1 μM Nucleosomes from HL-60 or from H2B-EGFP cells (preincubated with or without recombinant human PAD4). Samples were then lysed in a buffer containing 50mM Tris pH-8, 100mM NaCl, 1mM EDTA, 1% NP-40, 0.1% sodium deoxycholate, 0.1% SDS and 1x cComplete protease inhibitor cocktail (Sigma-Aldrich). MBP-H3 and MBP stimulated samples were incubated with Amylose Resin high flow (New England Biolabs) and Nucleosome stimulated lysates were incubated with a rabbit Histone H3 antibody (Millipore) and subsequently incubated with Sepharose Fast flow beads (Sigma-Aldrich). Samples were eluted in Laemmli buffer before being analyzed on a western blot using an anti-HA tag antibody.

Western blot analysis

Samples were resolved on a Criterion TGX precast gel (Any-KD, Bio-Rad Laboratories) and transferred on a Trans-Blot Turbo Midi PVDF membrane (Bio-Rad Laboratories) via semi-dry transfer. The membranes were then blocked in 5% BSA and incubated with anti-human myeloperoxidase (R&D), anti-human histone H3 (Millipore), anti-histone H3 citrulline R2+R8+R17 (Abcam), anti-human S100A8 (antibodies online), or anti-HA tag antibody (Abcam) and then incubated with HRP-conjugated secondary antibodies (Thermo scientific). Finally, the membranes were incubated with enhanced chemiluminescent substrate (ECL, ThermoFisher Scientific) and developed onto a photo film.

TLR reporter line assay

HEK-Blue reporter cell lines overexpressing human TLR2, TLR4 or TLR9 (as well as the respective parental lines) were obtained by Invivogen. These cell lines detect stimulants of the respective overexpressed receptors by induction of secreted embryonic alkaline phosphatase (SEAP). Cells were stimulated with recombinant Histone H3 (citrullinated with recombinant PAD4), preincubated with or without 100ng/ml of purified NET DNA, or 0.1 μM Nucleosomes purified from HL-60, EGFP-Nucleosomes purified from Cag::H2B-EGFP mice, 0.5ng/ml LPS (from Salmonella Minnesota R595, Enzo) or 1 μM CpG ODN2006 (Invivogen) or 100ng/ml FSL-1 (Invivogen). The levels of SEAP induction are determined with HEK-Blue Detection (Invivogen), according to the manufacturer's instructions and absorbance was monitored using a microplate reader (Fluostar Omega, BMG labtech).

Mice and atherosclerosis model

Female mice of 8–10 weeks old were fed for 6 or 16 weeks on a high fat diet (60% energy from fat, Testdiet). ApoE deficient mice were injected once a week for 6 weeks under high fat diet with 0.8mg/kg of the full IgG or the Fab fragment of the mouse anti-chromatin PL2-3 antibody (Losman et al., 1992) (prepared using the Pierce™ Fab preparation Kit by Thermo Fisher Scientific) or equivalent volume of PBS or vehicle (PBS passed through the Pierce™ Fab preparation Kit). Mice were sacrificed by terminal anesthesia and exsanguinated from the jugular vein for a terminal blood plasma sample that was collected in heparin-containing tubes. A PBS perfusion of the arterial system was then performed via the left ventricle of the heart. The heart was fixed with 4% PFA and then dehydrated overnight with 20% sucrose. Hearts were embedded in Optimum Cutting Temperature compound (OCT, VWR) and frozen in a dry ice cooled slurry of absolute Ethanol. The sections that comprised the aortic root as determined by the presence of the aortic valve leaflets, were serially sectioned on a Leica CM3050 S Cryostat at a thickness of 10 μm, collected and stored at –80°C. Sections were then stained with Oil Red O (Sigma-Aldrich) in 60% isopropyl alcohol and hematoxylin (RAL Diagnostics). Images were acquired using the Olympus Slidescanner VS-120 and analyzed using OlyVia software (Olympus). The relative plaque lesion area was calculated by using the averages from several consecutive sections measured using Adobe Photoshop and ImageJ software. For each section, the plaque area was analyzed proportionally to the total volume of the aortic root. For immunofluorescence staining of the atherosclerotic lesions, aortic root sections were first dried for 30 min at RT followed by incubation with 2% donkey serum, before being incubated with anti-histone 3 citrulline R2+R8+R17 (Abcam) and anti-mouse myeloperoxidase (R&D) as well as Alexa 647-conjugated anti-mouse Ly6G (Biolegend). Samples were counterstained with DAPI (ThermoFisher Scientific) before being mounted in ProLong Gold (ThermoFisher Scientific) and examined by confocal microscopy. Images were analyzed with ImageJ v2.0 software. Plasma samples from total blood of C57BL/6J wild-type (not on high fat diet) or APOE deficient mice after 6 weeks on high fat diet were analyzed for cytokine expression according to manufacturer's protocol for mouse IL-1β (ThermoFisher Scientific). For cholesterol and triglyceride levels, plasma samples were analyzed using the cobas c111 machine (Roche), following manufacturer's instructions.

For the *C. albicans* pulmonary infection, wild-type *C. albicans* (SC5314 clinical isolate) was cultured overnight in yeast extract peptone dextrose (YEPD) medium at 37°C before being subcultured in YEPD medium for 4 hours. Male and female wild-type and *CAG::H2B-EGFP* mice of 7–12 weeks were infected intratracheally with 1×10^6 *C. albicans* in PBS. To assess microbe load, animals were sacrificed 24 hours post infection, lungs were homogenized in PBS and were plated onto sabourad dextrose agar plates. To analyze cytokines in bronchoalveolar lavage (BAL), animals were sacrificed 24 hours post infection, lungs were rinsed with PBS and mouse IL-1β was measured by ELISA (ThermoFisher scientific).

Flow cytometry

CD14+ human monocytes, were stimulated with the indicated concentrations of H2B-EGFP nucleosomes for the indicated times or 0.5 μM MBP-H3 and 300ng/ml NET DNA for 2 hours. For cytotoxicity assay, samples were stained with LIVE/DEAD™ Fixable blue dead cell stain kit (Thermo Fisher) and then fixed with 4% PFA (Sigma). For TLR4 localization, CD14+ human monocytes were stained extracellularly, intracellularly or both with anti-human TLR4 (clone TF901, BD Biosciences) or Isotype control (mouse IgG1,k, clone MOPC-21, BD Biosciences) by using the Foxp3 staining buffer set (eBioscience). All data were acquired on the cell analyzer LSR Fortessa (BD) and analyzed using FlowJo software v10.

Immunofluorescence microscopy studies of TLR4 localization

5×10^4 human CD14 positive monocytes were stimulated with 0.5 μM of MBP-Histone H3 preincubated with or without 300ng/ml NET DNA. After 2 hours, cells were fixed in 2% paraformaldehyde and permeabilized with 0.5% Triton X-100 in PBS. Samples were blocked with 2% BSA and 2% Donkey serum in PBS and stained with antibodies against TLR4 (abcam), Rab5 (C8B1, Cell Signaling Technology) MBP (BioLegend). Samples were washed and stained with donkey anti-mouse Alexa -488, donkey anti-rat Alexa 568 and donkey anti-rabbit Alexa 647 (all from Invitrogen) before being counterstained with DAPI and mounted in ProLong Gold mounting medium on glass slides and examined by confocal microscopy using the Leica TCS SP5 confocal laser scanning microscope. Images were analyzed with ImageJ v2.0 software.

QUANTIFICATION AND STATISTICAL ANALYSIS

All quantitative data that has been collected from experiments is expressed as mean ± SD as indicated in the figure legends. All statistical analyses were performed on GraphPad Prism Version 7. The significance level for all comparisons was set at 0.05. The type of test employed for each comparison is described on the relevant figure legend. All tests employed were two-tailed. Annotations ns: $p > 0.05$, * $p \leq 0.05$, ** $p \leq 0.01$, *** $p \leq 0.001$, **** $p \leq 0.0001$.